The Innovation

Review

Features and futures of X-ray free-electron lasers

Nanshun Huang,[1,2] Haixiao Deng,[1,3,*] Bo Liu,[1,3] Dong Wang,[1,3] and Zhentang Zhao[1,3,*]

*Correspondence: denghaixiao@zjlab.org.cn (H.D.); zhaozhentang@zjlab.org.cn (Z.Z.)

Received: November 12, 2020; Accepted: March 14, 2021; Published Online: March 17, 2021; https://doi.org/10.1016/j.xinn.2021.100097

Graphical abstract

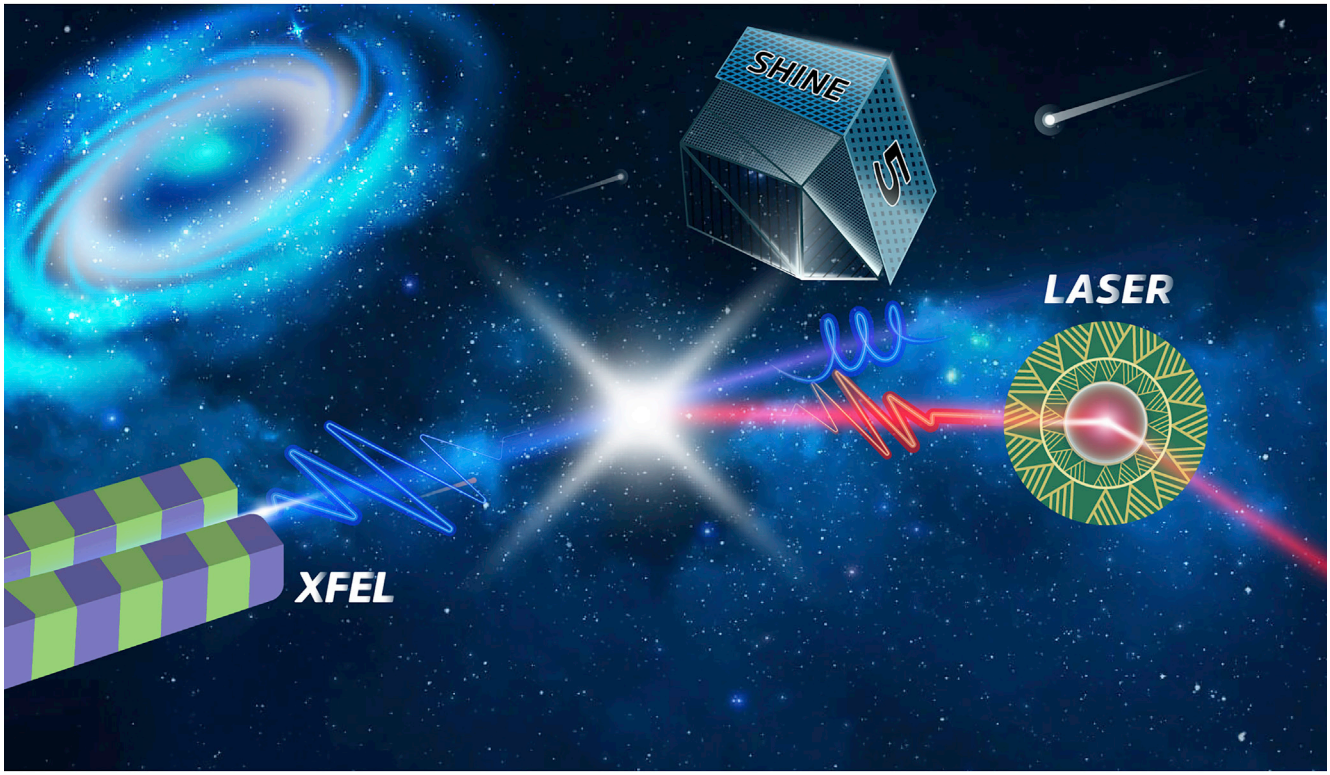

Public summary

- X-ray free-electron lasers (XFELs) generate X-ray by electrons flying through a periodic magnetic field.
- XFELs are the leading X-ray sources with ultra-high brightness and ultra-short duration.
- XFELs can be launched from either the shot noise of the electron beam or the seed.
- XFEL-laser collision is proposed to learn the nature of vacuum at SHINE.
- XFELs are being combined with intense lasers and synchrotron radiation light sources.

Review

Features and futures of X-ray free-electron lasers

Nanshun Huang,[1,2] Haixiao Deng,[1,3,*] Bo Liu,[1,3] Dong Wang,[1,3] and Zhentang Zhao[1,3,*]

[1]Shanghai Institute of Applied Physics, Chinese Academy of Sciences, Shanghai 201800, China

[2]University of Chinese Academy of Sciences, Beijing 100049, China

[3]Shanghai Advanced Research Institute, Chinese Academy of Sciences, Shanghai 201210, China

*Correspondence: denghaixiao@zjlab.org.cn (H.D.); zhaozhentang@zjlab.org.cn (Z.Z.)

Received: November 12, 2020; Accepted: March 14, 2021; Published Online: March 17, 2021; https://doi.org/10.1016/j.xinn.2021.100097

Citation: Huang N., Deng H., Liu B., et al., (2021). Features and futures of X-ray free-electron lasers. The Innovation **2(2)**, 100097.

Linear accelerator-based free-electron lasers (FELs) are the leading source of fully coherent X-rays with ultra-high peak powers and ultra-short pulse lengths. Current X-ray FEL facilities have proved their worth as useful tools for diverse scientific applications. In this paper, we present an overview of the features and future prospects of X-ray FELs, including the working principles and properties of X-ray FELs, the operational status of different FEL facilities worldwide, the applications supported by such facilities, and the current developments and outlook for X-ray FEL-based research.

INTRODUCTION

X-rays are of unique scientific importance, with the development of X-ray technologies among the most significant scientific achievements of the twentieth century. Following the discovery of X-rays by Roentgen, early applications focused on the particle-like behavior of X-rays, with the associated energy absorption manifested as shadow images that indicate material density. The most exciting application of X-rays relies on their diffraction, which can reveal the atomic structure of crystalline matter and forms the foundation of the field of crystallography. Following decades of further developments and breakthroughs, today macromolecular crystallography is established as the dominant structural characterization technique.[1] As of April 2020, the Protein Databank[2] comprised approximately 160,000 structural information entries, of which more than 140,000 were determined by X-ray diffraction. Moreover, high-intensity X-rays provide scientists in academia and industry with the opportunities to characterize materials spectroscopically, thus revealing specific details regarding the local bonding and structural environment of specific atoms. Today, X-rays are used not only for fundamental research, but also for applications in medicine, chemistry, and public security.

Although the knowledge obtained from X-ray experiments advanced steadily from the discovery of X-ray diffraction through to the mid-1970s, progress during this period was limited by the X-ray sources available, with X-ray tubes remaining essentially unchanged since 1912. The revolution in X-ray sources began with the inception of synchrotron radiation, with active research at synchrotrons and betatrons originally dedicated to high-energy and particle physics applications. Synchrotron radiation, the properties of which can be calculated very accurately, covers the spectral range from terahertz to hard X-rays, and provides significantly higher intensities than X-ray tubes. 1975 witnessed the construction of the first dedicated electron storage rings designed specifically to produce X-ray beams for studying photon science. These facilities are known as second-generation synchrotron sources, and generate X-ray beams using bending magnets, whereby electrons traversing a circular trajectory emit radiation in a broad spectrum. Another great leap forward occurred in the early 1990s, when the first third-generation light sources appeared.[3] Owing to the tremendous advances in accelerator physics and technology, these facilities are specifically optimized to make use of undulators and wigglers to generate X-ray beams that are approximately three orders of magnitude brighter than the second-generation synchrotron. Third-generation light sources are now available worldwide, with hundreds of beamlines and specialized instruments designed to satisfy specific research requirements. The development of synchrotron-based X-ray sources over the past 40 years has ushered in a modern age of X-ray science (leading to five Nobel Prizes since 1997). To increase X-ray brightness further, new storage ring lattices have been proposed at synchrotron radiation facilities, which are designed to reduce electron beam emittance to values close to the theoretical minimum for diffraction-limited light sources.[4]

Modern storage ring facilities provide bright X-ray beams with a high degree of spatial coherence. However, a minimum pulse duration of approximately 100 ps and the number of photons that can be focused on a small sample currently limit the development of novel X-ray applications. Significant strides have been made in the development of X-ray free-electron lasers (XFELs), considered to be next-generation light sources. Such devices can provide coherent laser-like X-ray pulses of femtosecond duration, which can be focused to intensities more than ten orders of magnitude higher than those produced at a third-generation facility. The development of FELs started with a concept proposed by Madey in 1971.[5] Subsequently, Madey's group[6] first demonstrated the feasibility of the FEL concept with an FEL oscillator in 1977. A combination of high-gain FEL concepts and accelerator techniques led to FELs operating in the X-ray regime being developed over the next 20 years.[7–17] The first soft X-ray FEL user facility, Free-electron LAser in Hamburg (FLASH) that was built at DESY, started operation in 2005,[18] while the first hard X-ray FEL, the Linear Coherent Light Source (LCLS) located at the SLAC National Accelerator Laboratory, began operations in 2009.[19]

In the past decade, LCLS has made great breakthroughs in various areas of basic research. Inspired by the tremendous success of LCLS, several XFEL facilities are currently in operation or under construction worldwide.[20–22] Offering various operation modes,[18–24] FEL facilities can generate X-ray pulses with photon energies up to 25 keV, sub-femtosecond pulse durations, pulse energies ranging from a few microjoules to several millijoules, and laser-like statistical properties. Furthermore, the repetition rate can be increased to a megahertz level by using superconducting linacs.[25–27] In short, XFELs can provide X-ray beams with unprecedented and raise the possibility of studying matter at atomic-level spatial scales and femtosecond timescales for the first time. Consequently, time-resolved measurements of molecular dynamics, exploring material properties under extreme conditions, and single-particle scattering imaging are now achievable goals.

The remainder of this review discusses the features and prospects of XFELs, with the remainder of the paper organized as follows. The next section considers the fundamentals of FEL theory, with particular focus on self-amplified spontaneous emission (SASE) FELs, externally seeded FELs, and cavity-based FELs. We then focus on the XFEL facilities in operation and under construction worldwide, while the next section discusses the various applications of XFELs, which we follow with a discussion of the current capabilities and future possibilities of XFELs. Finally, we present a short summary.

PRINCIPLES AND PROPERTIES OF XFELs

The FEL concept was introduced by Madey in 1971, and subsequently demonstrated via two FEL configurations: an FEL amplifier[28] and an

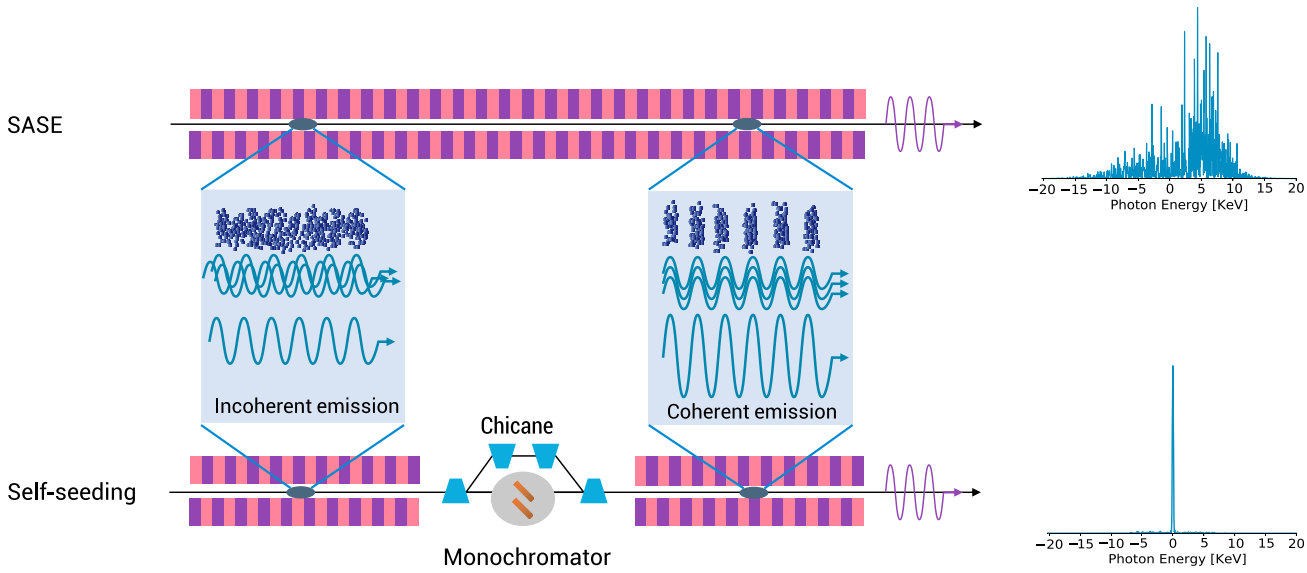

Figure 1. Schematic layouts for SASE and self-seeding Typical spectra corresponding to SASE and self-seeding are shown, respectively. The central part shows two types of electron distribution and the corresponding radiation emission. Incoherent radiation is emitted owing to the random phases of electrons at the entrance of undulator (left). If the electron beam exhibits micro-bunching at the radiation wavelength scale, a powerful coherent radiation pulse is generated (right). With increasing bunching, the fraction of coherent emission increases, leading to an exponential growth of radiation power along the undulators.

oscillator.[6] In the FEL amplifier, an external seed laser is required for amplification. In the absence of an external seed, spontaneous incoherent radiation is obtained. The oscillator can be started by using the noise generated by the spontaneous radiation; however, it needs an optical cavity to circulate the radiation pulse to achieve successive amplification with a small gain. The lack of good optical cavities operating in the X-ray spectral region precluded the possibility of realizing FELs at X-ray wavelengths via the oscillator configuration.

In fact, the requirement of an optical cavity was circumvented following the development of a theory for high-gain FELs during the late 1970s and the 1980s. In the high-gain regime, FELs are considered to start from spontaneous radiation, and reach saturation in a single undulator pass. This high-gain mode, named SASE FEL,[7,11] eliminates the need for an optical cavity and external seed. Moreover, as it does not depend on the radiation wavelength, this mode can operate at any wavelength. However, starting from the initial shot noise of an electron, the SASE FEL has a chaotic nature, and exhibits inherent spectral and intensity instabilities.

Beyond the SASE, externally seeded FEL can utilize frequency up-conversion techniques,[29] which manipulate electron beam phase space at the optical scale via commercially available UV lasers to obtain periodic charge density bunching at short wavelengths, and even X-ray wavelengths. Using this approach, the high-gain FEL process is triggered by a non-zero micro-bunching rather than an external seed directly. Therefore, this operating mode is not the amplifier but a harmonic generation of the seed laser. Consequently, the generated radiation is fully coherent, as its properties are characterized by the seed laser.

To date, SASE XFEL represents the best (and thus far, the only) alternative approach for generating hard X-ray laser beams. Externally seeded FELs can operate with better stability in the soft X-ray regime, while FEL oscillators are currently limited to the long-wavelength regime, e.g., terahertz, infrared, and UV. However, recent developments have shown that establishing optical cavities in the X-ray regime is feasible with the help of Bragg-reflecting crystals.[30] Overall, SASE is the most straightforward mode for XFEL operation. Here, we start by introducing the principles of SASE to provide a general understanding of the basic concepts in FEL, including the resonance condition, coherent emission, and micro-bunching.

Self-Amplified Spontaneous Emission

The physics underlying the FEL process can be explained using a simple model.[31] The fundamental FEL process involves the generation of spontaneous radiation through an undulator.[32] In a planar magnetic undulator, relativistic electrons move according to a "wiggling" (sinusoidal) trajectory, while the overall deflection of the electron beam is zero. Therefore, when traversing the undulator, the electrons are subject to acceleration and radiate electromagnetic waves, i.e., the spontaneous radiation. The resonant wavelength, at which the emitted radiation constructively interferes in the undulator, is expressed as

$$\lambda_h = \frac{\lambda_u}{2h\gamma^2}\left(1+\frac{K^2}{2}\right), \qquad \text{(Equation 1)}$$

where $h = 1, 2, 3, \ldots$, λ_u and K are the undulator period length and the dimensionless undulator parameter, respectively, γ is the relativistic energy of an electron, and h is the harmonic number of the radiation. A more detailed theoretical analysis reveals that only odd harmonic wavelengths of the radiation, i.e., $h = 1, 3, 5, \ldots$, are strongly emitted on-axis. The deflection parameter K is a measure of the angular excursion. From another perspective, Equation 1 shows that it is easy to generate radiation with the user-required wavelengths by adjusting either the energy of the electron beam or the undulator parameter K. For typical undulator parameters of $K \simeq 1$, the beam energy must be of the order of several GeV to reach sub-nanometer wavelengths.

The intensity of the radiation field emitted by many electrons in an undulator is written as

$$\left|\sum_{j=1}^{N_e} E_0 e^{i\omega t_j}\right|^2 = E_0^2 N_e + E_0^2 \left|\sum_{j=1}^{N_e}\sum_{k=1}^{N_e} e^{i(\omega t_j + \omega t_k)}\right|^2, \qquad \text{(Equation 2)}$$

where E_0^2 is the radiation intensity from one electron, and the total number of electrons is $N_e \gg 1$. For electrons with random longitudinal positions, the second term is much smaller than N_e and considered to be negligible. In this case, the electric fields corresponding to the waves generated by each electron are superimposed at random and the intensity is proportional to N_e. This is called incoherent radiation and is illustrated in the left colored panel of Figure 1. For electrons with correlated phases $t_j \approx t_k$, the second term is considerable and the intensity becomes proportional to N_e^2. This is called coherent radiation and is illustrated in the right colored panel of Figure 1.

As the spontaneous radiation of many electrons has no phase correlation, the total emitted intensity is proportional to the electron number N_e.

This imposes a limitation on the radiation intensity generated by synchrotron radiation light sources. To increase the intensity significantly, phase correlation must be incorporated. This means that the electron sources must be bunched periodically at the resonant wavelength λ. Such micro-bunching can be obtained via FEL amplification, which leads to a longitudinal distribution of electrons that is modulated at the radiation wavelength λ.

The micro-bunching results from the interaction between the relativistic electron beam and radiation field in the periodic magnetic field of the undulator. The mechanism of FEL amplification can be summarized as three basic processes:[33,34]

1) The interaction of electrons with the radiation field causes the energy of the electron beam to be modulated.
2) This energy modulation evolves into longitudinal density modulation (micro-bunching) at the scale of the resonant radiation wavelength λ, as determined by Equation 1. This is due to the path length difference between trajectories of electrons with different energies.
3) The micro-bunching results in the amplification of the radiation field through coherent emission.

It is straightforward to show that FEL amplification is a positive feedback loop, whereby a larger intensity leads to enhanced energy modulation and, thus, more bunching. As a result, the radiation intensity can grow exponentially up to a limit of N_e^2, thereby enabling a high-gain single-pass FEL with a sufficiently bright electron beam and a sufficiently long undulator. It should be noted that the N_e^2 limit is reached in cases of extreme micro-bunching, in which all electrons have the same emission phase and the radiation is fully coherent. As discussed above, the most important quantity in this process is the micro-bunching. And the FEL amplification cannot continue indefinitely and eventually saturates as the micro-bunching reaches a maximum.

For high-gain FEL theory with a one-dimensional (1D) limit, the FEL equations describing the motion of electrons and the evolution of the radiation can be written in a universal form that depends solely on the FEL parameter, ρ.[11,34] This quantity is a function of the undulator and electron beam characteristics and does not depend explicitly on the radiation wavelength. The electromagnetic power before reaching saturation is given, approximately, by

$$P \approx \frac{1}{9} P_0 e^{z/L_g}, \qquad \text{(Equation 3)}$$

where the power gain length is $L_g = L_{g0}(1+\Lambda)$. $L_{g0} = \lambda_u/4\pi\sqrt{3}\rho$ is the 1D power gain length of a monoenergetic radiation. Λ quantifies the degradation effects, such as diffraction. ρ is defined as

$$\rho = \left[\frac{1}{16}\frac{I}{I_A}\frac{K^2[JJ]^2\lambda_u^2}{\gamma_0^3\sigma_x^2 4\pi^2}\right], \qquad \text{(Equation 4)}$$

where $I_A = 4\pi\epsilon_0 mc^3/e \approx 17kA$ is the Alfvén current and $2\pi\sigma_x^2$ is the cross-sectional area of the electron beam. $[JJ]$ is the Bessel function factor. For a planar undulator, $[JJ] = J_0(\xi) - J_1(\xi)$ with $\xi = K^2/(4+2K^2)$. For a helical undulator, $[JJ] = 1$. For XFELs, such as LCLS and SACLA, the FEL parameter ρ typically has a value of approximately 0.001, corresponding to a gain length of several meters, while the total undulator length is over 100 m.[34,35] Moreover, the FEL parameter can summarize the radiation characteristics. For example, another important parameter, the saturation power, is a fraction of the value of ρ that corresponds to the electron beam power P_{beam}:

$$P_{\text{sat}} \simeq \rho P_{\text{beam}}. \qquad \text{(Equation 5)}$$

Thus, the FEL parameter describes the efficiency of the energy transfer from the electrons to the radiation field. In addition, the relative bandwidth is approximately equal to the FEL parameter: $\Delta\lambda/\lambda \approx \rho$. By combining the power and bandwidth formulae, the number of coherent photons per electron also becomes related to ρ.

Note that the FEL amplification can be triggered by an external seed or by non-zero micro-bunching at the undulator entrance. When the initial field is not zero and the initial bunching and energy modulation are zero, the FEL acts as an amplifier. When the initial condition of the system involves non-zero bunching due to the inherent fluctuations in electron positions at the undulator entrance, this system acts as a SASE FEL,[11,34] for which the initial radiation is produced via spontaneous radiation. In particular, for X-rays with sub-nanometer wavelengths, where no practical laser sources can provide a suitable initial field, the SASE mode is the most straightforward method of FEL operation.

Some proof-of-principle experiments investigating SASE were conducted at a wavelength of 16 μm at the University of California, Los Angeles.[17] Scientists in Hamburg then recognized the opportunity to build an extreme UV (EUV) FEL facility known as FLASH.[18] This pioneering achievement inspired the construction of soft X-ray FELs and the LCLS. To date, all hard X-ray FELs in operation are based primarily on the SASE mode, including LCLS, SACLA, PAL-FEL, and SwissFEL.

The radiation produced by the SASE mode has a coherent transverse form due to the gain-guiding effect.[36] However, starting from shot noise, SASE FEL radiation behaves chaotically owing to the stochastic nature of spontaneous undulator radiation emissions. Significant efforts have been invested in enhancing the temporal coherence and achieving an effectively controlled bandwidth of the SASE X-ray spectrum. Several schemes have been proposed for this, such as self-seeding operation in soft and hard X-ray regimes,[37] high-brightness SASE,[38] improved SASE,[39] purified SASE,[40] and harmonic lasing self-seeded FELs.[41] The main experimental results obtained for self-seeding[42] show that the spectral bandwidth of SASE can be reduced by more than an order of magnitude, with a typical bandwidth of approximately 0.4–0.5 eV at 8–9 keV, which is near Fourier-transform limited and 50 times narrower than the initial SASE results.

In general, a self-seeded FEL consists of three parts, as shown in the bottom panel of Figure 1. The first part is a short undulator, which can generate SASE FEL pulses with a low pulse energy. In the second part, the bandwidth of the generated SASE radiation pulse is reduced by a monochromator, while the electron beam is delayed by a chicane. Micro-bunching of the electron beam, built up in the previous SASE process, is destroyed by this delay. Then, the third part is an FEL amplifier in which the filtered coherent X-ray pulse is amplified to reach power saturation by interacting with the "refreshed" electron beam. For X-ray wavelengths, self-seeded FELs can be realized in three ways: grating monochromators,[37,43] micro channel-cut crystal monochromators,[44] and single-crystal or "wake" monochromators.[42,45] This solution can increase the spectral brightness by an order of magnitude relative to that obtained form the SASE XFEL. However, the self-seeding scheme suffers intrinsically from low seed power as a result of attempting to preserve the electron beam properties important for lasing. Furthermore, it depends fundamentally on the noisy SASE process leading to large (~100%) seed power fluctuations. For the same setup, if the monochromator is replaced by an atomic gas, the inner-shell laser pumped by an upstream XFEL pulse can be used as the monochromatic seed for a downstream undulator that generates fully coherent XFEL pulses.[46]

Externally-Seeded FELs

In addition to the SASE XFEL method, several external seeding schemes have been developed to produce fully coherent X-ray pulses with commercially available seed sources. These schemes manipulate optical-scale electron beam phase space to generate micro-bunching at the harmonic wavelength of the seed, thereby circumventing the need for a seed source at short wavelengths and triggering high-gain FEL amplification in the undulator. In general, this manipulation focuses on the (z, p) phase space, where p denotes the dimensionless energy deviation and z is the longitudinal position. To manipulate the (z, p) phase space, an external seed laser is required to modulate the electron energy through an undulator. Then, the energy modulation is converted to density modulation via a dispersive element. These

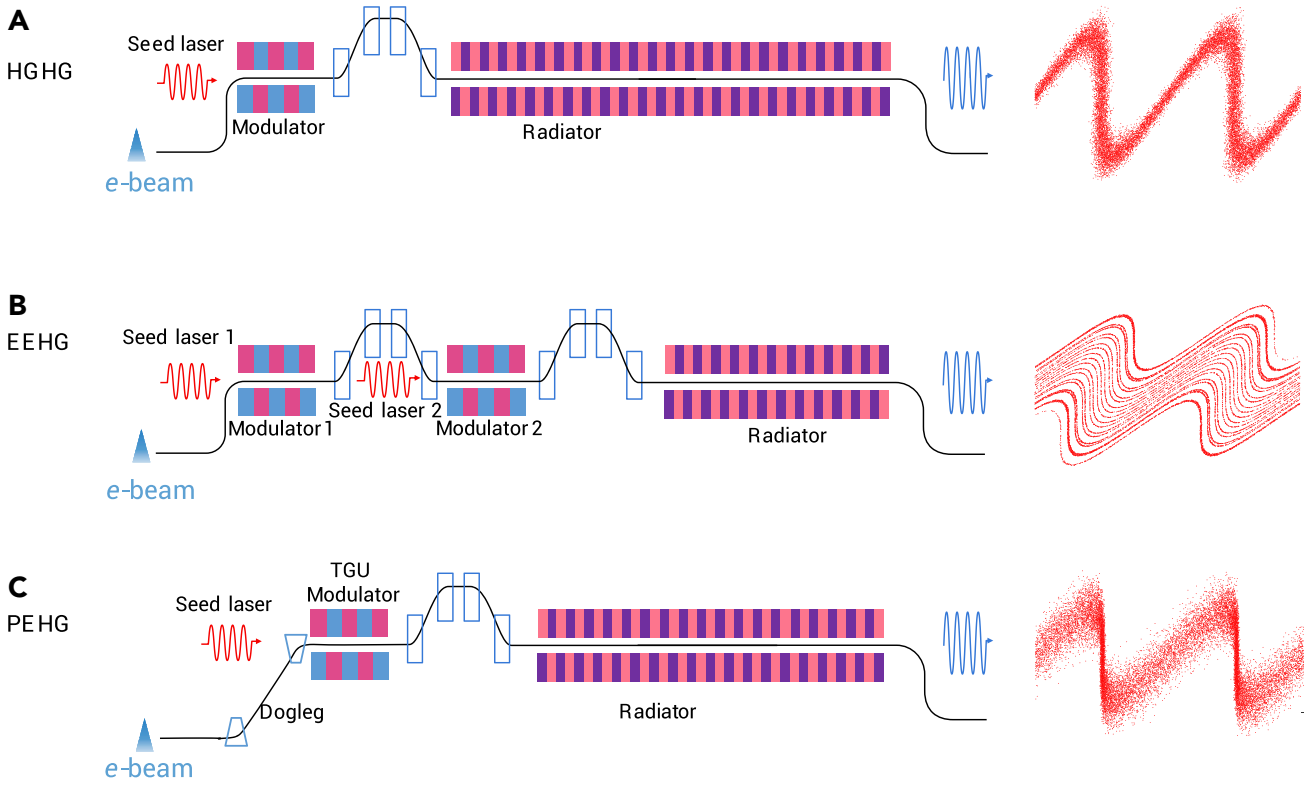

Figure 2. Schematic layouts for various external seeding techniques (A) HGHG, (B) EEHG, and (C) PEHG.

approaches are now being considered by many research groups for developing soft X-ray FELs.

The first scheme based on an external seed laser is high-gain harmonic generation (HGHG).[29,47] The layout of the HGHG scheme is shown in Figure 2A. The HGHG scheme comprises three sections. The first part, known as the modulator (an undulator with large λ_u), involves a seed laser interacting with the electron beam to impose a small energy modulation. Then, the electron beam is transferred through the second part, known as dispersion section, whereby the energy modulation is converted into spatial density modulation. Finally, the micro-bunched electron beam passes through the third part, known as the radiator (long undulator), in which the electron beam resonates at the harmonic frequency of the seed laser, thus causing the electron beam to emit a coherent signal at the harmonic frequency, which is then amplified exponentially to the saturation threshold by the radiator. Currently, there are two FEL user facilities whose operation is based on HGHG.[23,24] However, significant bunching at higher harmonics is usually needed to strengthen the energy modulation in HGHG, which results in the degradation of the amplification process in the radiator.

Improvements to the harmonic conversion efficiency of externally seeded FELs based on the HGHG scheme are limited by the slice energy spread of the electron beam. An alternative scheme, namely echo-enabled harmonic generation (EEHG), was proposed in 2009,[48] with a corresponding schematic shown in Figure 2B. In EEHG, there are two modulators and two dispersion sections: (1) the electron beam interacts with the seed laser in the first modulator, which introduces a small energy modulation to the electron beam; (2) the modulated electron beam arrives at the first dispersion section, which has a strong dispersion effect that causes a fine energy band in the (z,p) phase space of the electron beam; (3) then, this electron beam interacts with another seed laser, imprinting a second small energy modulation on the energy band; (4) next, the electron beam is passed through the second dispersion section, which converts the energy modulation into the space density modulation; and (5) finally, the density-modulated electron beam is passed through a long undulator to amplify a coherent signal such that it reaches saturation at high harmonics of the two seed laser frequencies. The configuration of EEHG FELs is flexible and complex, in which the optimization of the bunching factor is essential to enable its full performance. The optimization factor includes two modulation amplitudes of the modulators and the dispersive strength of each chicane.

A proof-of-principle experiment demonstrating EEHG was performed in 2010 at the Next Linear Collider Test Accelerator: Research of Dielectric Laser Acceleration.[49] The first lasing via an EEHG FEL at the third harmonic of the two seed frequencies was conducted in 2012 using the Shanghai deep UV free-electron laser (SDUV-FEL).[50] Following this experiment, the EEHG FEL method has attracted significant attention because of the advantages it offers, with many experiments subsequently performed at higher harmonics.[51–53] The operation of the first soft X-ray EEHG FEL was demonstrated at FERMI in 2019.[54] In this experiment, 7.3 nm soft X-rays, that is, the 36th harmonic of two identical seed laser wavelengths, were amplified to saturation. The stability of the spectrum and the intensity can be seen in Figure 3. In addition, the saturation of the 11th harmonic and lasing via the 30th harmonic of the EEHG setup has been achieved at the Shanghai Soft X-ray FEL Facility (SXFEL).

However, generating ultra-high harmonics (larger than 100 harmonics) using the conventional EEHG scheme is difficult owing to incoherent synchrotron radiation, coherent synchrotron radiation, and intra-beam scattering effects. To overcome these effects, selecting an EEHG parameter of $n = -4$ to generate the 150th harmonic for single-stage EEHG was first proposed in (Zhou et al.[55]). The $n = -4$ value indicates the use of the fourth-order modes of the fundamental bunching. The analysis shows that, by choosing the fourth-order modes of the EEHG scheme, it is possible to produce coherent X-rays at the 150th harmonic directly from a UV seed laser source. This was demonstrated in part by the FERMI group in 2019, when they observed the 101th harmonic of EEHG at $n = -4$, corresponding to the generation of a highly coherent signal with a wavelength of 2.6 nm.

Phase-merging enhanced harmonic generation (PEHG) is another physical mechanism that promises to provide strong enhancement of the frequency

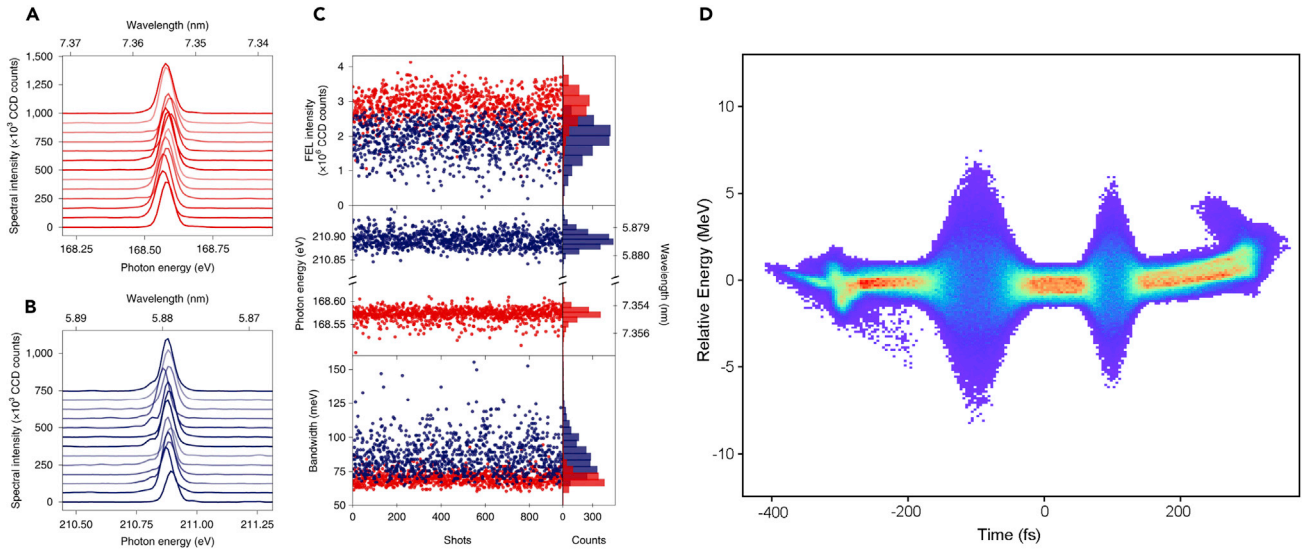

Figure 3. Soft X-ray EEHG experiments and fresh bunch technique (A–C) Experimental analysis of the FEL spectrum in the EEHG mode at $\lambda = 7.3$nm (~ 169 eV) with $h = 36$ and $\lambda = 5.9$ nm (~ 211 eV) with $h = 45$, where h is the harmonic number. (D) Schematic of the fresh bunch technique for the cascading harmonic generation scheme at SXFEL. Different fractions of the electron beam are used for lasing in different stages, implying that a single beam can be used for multi-stage harmonic generation. Reprinted with permission from the Copyright Clearance Center: Springer Nature, Nature Photonics (Ribič et al.[54] Coherent soft X-ray pulses from an echo-enabled harmonic generation free-electron laser), Copyright (2019).

up-conversion efficiency in seeded FEL configurations.[56,57] Figure 2C shows the schematic layout of PEHG. Before entering the transverse gradient undulator (TGU), the electron beam passes through the dogleg; therefore, electrons with different energies are dispersed into different transverse positions. In the TGU modulator, the electron beam undergoes a gradual energy modulation from the external seed laser. Meanwhile, electrons in different transverse positions experience different undulator K values, resulting in different travel path lengths. Furthermore, if the gradient of the TGU modulator, together with the transverse dispersion of the dogleg, is chosen properly, in regions around the zero-crossing of the seed laser, electrons with equivalent energy gradually travel to the same longitudinal phase. This phenomenon results in phase-merging. As in other seeded schemes, the electron beam is passed through a dispersive chicane to implement density modulations, which contain significantly enhanced high harmonic signals of the seed laser.

The electron beam phase spaces that emerge after passing through the dispersive chicane are illustrated in the left panel of Figure 2. The difference in the phase space manipulation of each scheme can be found. While other harmonic generation schemes only manipulate the longitudinal phase space of the electron beam, the fundamental physical mechanism of PEHG is transverse-longitudinal phase space coupling. Considering that most electrons are concentrated around the same phase, the density modulation and frequency up-conversion efficiency in PEHG are significantly enhanced, with this property utilized to generate fully coherent short-wavelength radiation at very high harmonics of the seed. In accordance with a Gaussian energy distribution, the coherent bunching factor scales as $0.67/h^{1/3}$ for PEHG,[56] as compared with $0.39/h^{1/3}$ for EEHG.[48]

Further studies indicate that the optimal bunching factor of PEHG is determined by a combination of factors, which includes the initial transverse beam size, the initial transverse beam divergence, and the practical lattice configuration.[58] These factors influence the transverse positions of the electrons in the TGU, and thus impact the phase-merging effects and the final bunching results greatly. The layout of the PEHG scheme can be varied. For example, the TGU modulator can be replaced by a normal modulator for energy modulation and a separate TGU for implementing phase-merging effects.[57] Moreover, the phase-merging effects of the TGU can also be fulfilled by utilizing a wavefront-tilted seed laser,[59] magnetic dipole,[60] or by using the natural transverse gradient of a normal undulator.[61,62]

The requirement for FEL amplification of the beam energy spread makes it impossible to generate hard X-rays via single-stage HGHG or EEHG. Therefore, the multi-stage harmonic generation schemes have been proposed in which an FEL pulse generated by an intermediate radiator is used as the seed laser for the harmonic generation stage via the "fresh bunch" technique.[63] In these schemes, the temporal duration of the seed is shorter than the electron beam pulse duration, thereby enabling the seed to overlap with a "fresh" electron beam region that has not been affected by FEL interactions in the previous stage, as shown in the bottom plot of Figure 3. Analysis within the framework of idealized models suggests that two-stage HGHG can produce fully coherent soft X-rays, while two-stage PEHG has the potential to reach the hard X-ray regime.[64] The first cascaded HGHG scheme using the fresh bunch technique was demonstrated at the SDUV-FEL, where higher photon energies were obtained.[65] The two-stage HGHG scheme has also been adopted by FERMI and SXFEL as the baseline for FEL operation.[24,66] Furthermore, a 10th × 3th EEHG-HGHG cascading scheme, which can generate an 8.8 nm FEL pulse using a 266 nm seed laser, has been demonstrated successfully at SXFEL.

Cavity-based XFELs

Cavity-based FELs are considered highly promising candidates for generating fully coherent FEL pulses. In such FELs, X-ray pulses that are stored and recirculated in an X-ray optical cavity are amplified via interactions with fresh electron bunches when passing through undulators. Cavity-based FELs include XFEL oscillators (XFELOs)[67] and X-ray regenerative amplifier FELs (RAFELs),[68] both of which use the same fundamental techniques and components to realize their full capability. In general, these solutions require a high repetition rate electron bunch together with an undulator to provide gain and a crystal cavity to circulate and store the X-ray pulses. Following progress in the crystal optics and accelerator techniques required for an XFELO, such as defect-free diamond crystals and high repetition rate electron beams from superconducting linacs, XFELOs have now become technically feasible.

A schematic of the XFELO system is shown in Figure 4. An undulator of appropriate length is mounted inside the X-ray cavity, with relativistic electron beams delivered from a superconducting linac. In the undulator, the electron beam amplifies the recirculated X-ray pulse as the FEL process occurs. Equipped with a low coupling-out X-ray cavity, XFELOs work in the low-gain regime, where the single-pass gain is typically less than 1. Thus, they require hundreds of round trips before power saturation occurs. The X-rays can be coupled out of the X-ray cavity through transmission via a crystal mirror.

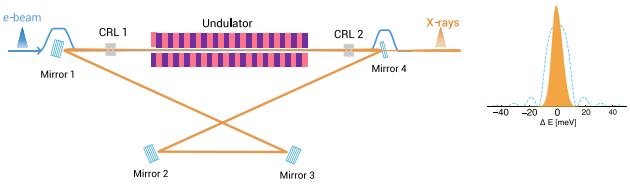

Figure 4. Schematic layout of XFELO The right plot shows a typical XFELO spectrum with an FWHM bandwidth of meV level, which is three order of magnitude narrower than the high-gain SASE XFELs..

An alternative method for extracting the intra-cavity X-ray pulse by inserting an additional mirror has been proposed in Shvyd'ko.[69] The transverse optical mode of an XFELO is controlled by external focusing elements, such as multilayer curved mirrors or compound refractive lenses. For Bragg crystals, diamond is the material of choice used to form X-ray cavities because of its high reflectivity, mechanical properties, and excellent thermal stability. Using diamond crystals extends the range of photon energies from 5 to 25 keV and provides 8 GeV electron bunches at a repetition rate of ~ 1 MHz, with these parameters typically provided at LCLS-II-HE and the Shanghai high repetition rate XFEL and extreme light facility (SHINE).

The RAFEL has the same structure as the XFELO, including a high repetition rate electron beam, a relatively long undulator, and an X-ray optical cavity to provide feedback. However, unlike the XFELO, which operates in the low-gain regime with a low-output coupling cavity, the RAFEL is a high-gain FEL that operates in a high-output coupling cavity. Thus, it requires only a few round trips to reach saturation. When considering the potential challenges associated with cavity design, the RAFEL offers many other unique advantages over oscillators. For example, the high-gain property can provide additional compensation for relaxing the X-ray-induced degradation of the cavity optics as the small number of round passes should relax longitudinal alignment tolerances compared with the XFELO. Owing to the gain-guided effect, the dominant transverse mode is defined by the FEL gain. Therefore, the optical cavity is used mainly for recirculating the X-ray pulse to feedback the FEL amplification. An experiment to generate double electron bunches in the Cu-linac at LCLS has been designed to measure the two-pass gain as well as the cavity ring-down efficiency for the high-gain RAFEL scheme.

The defining merit of cavity-based XFEL sources is the significantly improved longitudinal coherence relative to high-gain SASE XFELs. For example, the bandwidth of the XFELO pulse can be as small as a few meV, while its temporal duration is a few hundredths of a femtosecond (i.e., nearly transform limited). In contrast, radiation from SASE XFELs is characterized by ultra-short temporal durations that can be smaller than a femtosecond, while its spectral bandwidth reaches a few tens of eV (i.e., far away from the transform limit). Therefore, an XFELO can provide a high spectral photon density, while a SASE XFEL generates a high temporal photon density. In addition, cavity-based XFELs produce highly stable X-ray pulses with shot-to-shot fluctuations of approximately 1%, while high-gain SASE XFELs and self-seeded XFELs suffer from poor pulse-to-pulse stability.

The physics of cavity-based XFELs, including the FEL process and Bragg diffraction, is more complicated than that of a single-pass high-gain FEL. Thus, numerical simulations are typically used to study these systems. Recently, a 3D Bragg diffraction code called BRIGHT,[70] which can be used with the time-dependent FEL code and optical propagation code, was developed to enable fully 3D XFELO simulations. In addition, the crystal mirrors, which are exposed to intense X-ray beams in the optical cavity, are subject to thermal deformations. A new approach has been developed, that utilizes a dedicated Bragg reflection physical process in the GEANT4 software package to obtain precise information on the absorption of XFELO pulses in the crystal.[71] With the help of external finite element analysis software, this method provides a valuable tool for analyzing the thermal load of the mirrors in an XFELO. In addition, a simplified 1D theoretical XFELO model has been established for the fast optimization of the single-pass gain and spectrum in XFELO systems.[72] In addition, to avoid the need for the X-ray focusing elements used in the conventional XFELO configuration, a gain-guided XFELO has been proposed.[73] The FEL gain of the electron beam is used to focus the X-rays transversely, thus maintaining mode stability.

In terms of flexibility, XFELOs have the potential to be expanded for use in a wealth of applications. To serve the demands of high-photon energy experiments, XFELOs can extend the photon energy coverage by running the XFELO at a higher harmonic,[74] or the XFELO output can be used as the input seed for an external HGHG system.[29,75–78] Such a system was studied with a view to extending the photon energy by a factor of 5 to 40–60 keV. In addition, to generate high-power X-ray pulses reaching the terawatt level, XFELOs can also be used as the seed in master oscillator-power amplifier (MOPA) configurations.[79] The tapering section further increases the pulse intensity owing to the high degree of coherence. In addition to the MOPA configuration, a gain cascading scheme has been proposed for increasing the maximum energy conversion efficiency of an XFELO with a constant undulator parameter.[80] The gain cascading scheme, which controls the delay elements between the undulator stages to allow electron beam lasing at various locations inside different undulators, can increase the energy extraction efficiency and output peak power by shortening the undulator length at each stage. Furthermore, by utilizing a crossed-planar undulator, an XFELO can generate polarization-controllable fully coherent hard X-ray pulses, with a polarization degree of 99% and a polarization switching rate of 20 kHz.[81] This scheme consists of two cross-configured planar undulators in which two orthogonally linearly polarized field components are generated separately. By inserting a fast phase shifter between the two undulators, the phase difference between the two linearly polarized components can be controlled. Recent studies have shown that XFELOs can generate light with orbital angular momentum without requiring any external mode-conversion optical elements.[82]

In recent decades, significant progress in superconducting linacs using high repetition rate XFELs[25–27] and in achieving defect-free crystals[30] has paved the way for the eventual construction of cavity-based FELs. Moreover, by extending the idea of crystal cavities beyond FELs, related schemes have been proposed for producing intense, fully coherent, transform-limited pulses, such as a population inversion X-ray laser oscillator,[83] which uses a liquid jet as the gain medium and SASE XFEL pulses as pumps. In this proposed device, the pump pulse impinges on a liquid jet sample, where it initiates population inversion followed by amplified spontaneous emission. The emitted signal, which is recirculated in a Bragg crystal cavity, then provides the seed for stimulated emission and is amplified in each subsequent pass until it reaches saturation (this typically requires four to eight passes). At saturation, the generated pulse is outcoupled by tuning one of the crystal mirrors to an off-Bragg condition.

OVERVIEW OF XFEL FACILITIES WORLDWIDE

In a typical XFEL facility, a linear accelerator is used to produce bright electron beams, which are then delivered to multiple undulator lines to generate intense radiation with dedicated properties for different experiments and applications. A switchyard is inserted between the accelerator and the undulator lines. Thus, the evolution of XFEL facilities is expected to be focussed on techniques for improving accelerator performance and the generation of photon beams with unprecedented and exotic properties. By developing flexible and unique XFEL techniques, the customizability of photon beams can be extended, thereby satisfying a tremendous diversity of scientific applications covering various aspects of chemistry, physics, and biology.[84,85]

Figure 5 shows a timeline detailing the year of first lasing for various XFEL facilities worldwide. The development of these facilites and the technological advancements have been primarily centered on shortening the generated wavelength to the hard X-ray region and increasing of the average power to several hundred watts. In the next section, we briefly review the characteristics and performance parameters of each facility in detail. The features and specialties of key experimental stations are also included. A summarized dataset can be found in Table 1.

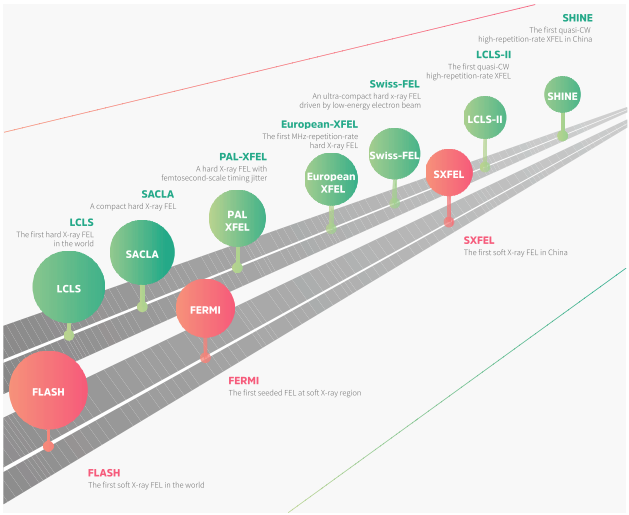

Figure 5. Timeline indicating the first lasing of various FEL facilities worldwide.

Copper linac-based XFEL facilities

One of the most exciting and impressive milestones in the development of XFELs was the successful operation of the first hard X-ray FEL facility, LCLS, in 2009,[19] which provides XFEL pulses with extremely high brilliance and excellent transverse coherence. At LCLS, extremely high-brightness electron beams of 13.6 GeV are generated in a normal conducting linear accelerator with a typical repetition rate of 10–120 Hz, while a 0.15 nm SASE mode FEL is generated in the 132-m-long fixed-gap undulator system. LCLS routinely produces X-ray pulses with durations shorter than 200 fs, photon energies ranging from 0.28 to 12.8 keV, and 10^{12} photons per pulse at 8 keV. An adjustable low- and high-energy mirror system downstream directs the soft X-rays to the experimental stations for atomic, molecular, and optical science, soft X-ray research, and X-ray pump-probe, and hard X-rays into four other stations, including X-ray correlation spectroscopy, macromolecular femtosecond crystallography, coherent X-ray imaging, and matter in extreme conditions. Benefiting from the unique and incomparable performance far beyond those of the other contemoraryfacilities at the time, cutting-edge experiments and methods were developed and established at LCLS,[86] resulting in the publication of over 1,500 papers in the past decade.

Two years later, the SACLA facility in Japan achieved its first lasing with an unprecedented short wavelength of 0.06 nm for the SASE mode.[20] Advanced technologies, such as a thermionic gun with a cesium boride cathode, a C-band accelerator structure, and in-vacuum undulators with variable gaps, were all successfully manufactured and utilized for the first time in the SACLA XFEL facility. Benefiting from the application of these technologies, SACLA delivers sub-Ångstrom X-ray pulses with an 8.5 GeV electron beam, which makes SACLA the most compact XFEL facility to date. Compared with LCLS, the overall size is approximately three to five times smaller for the same FEL tuning range, enabling a significant reduction in construction and operating costs. SACLA can deliver FEL pulses via three beamlines simultaneously, namely a spontaneous radiation beamline (BL1), which was upgraded to a soft X-ray FEL in 2017, and two hard X-ray FEL beamlines (BL2 and BL3), which typically deliver FEL pulses from 4 to 20 keV. The major applications of BL1 include the observation of nonlinear optical processes in gaseous atoms and molecules, and the evaluation of ultrafast phenomena in solid-state materials. There are two experimental stations at BL2, which focuses on biology-oriented experiments, such as protein crystallography and coherent diffraction imaging (CDI), with the other station tackling high-energy density science with a high-power femtosecond laser system. BL3 is a more comprehensive beamline, with the ability to accommodate experiments from different subject areas, including structural biology, ultrafast physics, chemistry, and X-ray quantum optics. At SACLA, several user groups can run experiments concurrently thanks to the multiple-beamline operation, amassing a total user beam time of approximately 5000 h per year.[87]

After the first decade of user operation, XFELs have been demonstrated as a dedicated light source in the research of spatial and temporal scales of atomic and molecular motion that underpin many processes, such as energy conversion and storage. Potential for further cutting-edge scientific research is supported by two room temperature FEL facilities, namely the SwissFEL[22] and the PAL-XFEL,[21] which joined the thriving hard X-ray FEL community in 2017.

The overall goal of the SwissFEL is to provide a compact facility that produces 0.1–5.0 nm FELs with pulse durations ranging from 1 to 20 fs.[22] The electron beam is accelerated to 5.8 GeV in a normal conducting C-band linear accelerator, and two undulator branches, Athos and Aramis, are utilized to generate soft and hard X-rays, respectively. The SwissFEL focuses on high economic impact research, such as materials science, chemistry, and biology. Three experimental stations, Alvra, Bernina (active), and Cristallina (under construction), were proposed for the initial phase of the Aramis beamline. Alvra focuses primarily on X-ray spectroscopy and serial femtosecond crystallography (SFX), while Bernina is designed to perform time-resolved hard X-ray pump-probe diffraction and scattering experiments in condensed matter systems. The soft X-ray beamline Athos is under construction and scheduled to commence user operation later this year.

PAL-XFEL, in Korea, first conducted successful lasing in 2017.[21] It consists of an 11 GeV normal conducting linear accelerator, and can generate X-ray FELs ranging from 0.1 to 6 nm. The facility has space for five undulator lines in total; specifically, three hard X-ray undulator lines and two soft X-ray undulator lines. Currently, one hard and one soft X-ray line are installed and operational. The most remarkable feature of PAL-XFEL is the 20 fs timing jitter of the intense X-ray photon beam, which is achieved consistently owing to the use of a state-of-the-art electron linear accelerator design and electron beam-based alignment. The optically pumped phonon modulation of Bi(111) has been performed without any XFEL-related optical jitter correction. At present, the nanocrystallography and imaging station and the X-ray scattering and spectroscopy station both utilize the hard X-ray beamline, which provides a photon energy range of 2–12 keV, with a narrow bandwidth of 2.1–20 eV. The soft X-ray scattering and spectroscopy station provides soft X-rays ranging from 0.25 to 1.2 keV at a repetition rate of 60 Hz with a pulse duration of approximately 90 fs.

FERMI@Elettra is the first seeded XFEL user facility.[23] The electron bunch, which has a beam energy of 1.5 GeV and repetition of 50 Hz is delivered into two different APPLE-II type undulator lines, FEL1 and FEL2, for vacuum UV and soft X-ray generation, respectively. A 20–65 nm highly coherent and stable FEL pulse has been achieved using the principle of single-stage HGHG in FEL1,[23] while a wavelength of 4.3 nm has been achieved using two-stage cascaded HGHG in FEL2.[66] Another unique feature of FERMI is the capability to produce an FEL with variable polarization (from completely linear to completely circular) using helical undulators, which is particularly important for soft X-rays owing to the lack of a practical phase retarder. A photon analysis delivery system is located downstream of the undulator line to characterize, manipulate, and deliver the FEL radiation to the final experimental stations, which include stations for CDI, absorption and elastic scattering from materials under extreme conditions, gas-phase and cluster spectroscopy, inelastic and transient grating spectroscopy, terahertz applications, and magneto-dynamics.

Inspired by the rapid construction and commissioning of XFELs worldwide, China has invested significant effort into the development of XFEL technology, resulting in the SXFEL,[24] which is a two-phased FEL, i.e., with a proposed transition from a test facility to a user facility. It aims to cover photon wavelengths ranging from 10 to 2 nm. During the test phase, the flexible configuration of SXFEL is designed to facilitate various seeded FEL experiments, e.g., the combination of EEHG and HGHG has been designed to pursue very stable spectral properties and ultra-high harmonic up-conversion efficiency. As of the middle of 2020, 8.8 nm FEL lasing experiments with 6th × 5th HGHG-HGHG cascading, 10th × 3th EEHG-HGHG cascading,

Table 1. Major parameters for worldwide X-ray FEL facilities

Facility	Beam energy (GeV)	Photon energy (eV)	Repetition rate (Hz)	Pulse duration (FWHM) (fs)
FLASH	0.35–1.25	14–620	4×10^3 to 10^6	10–200
LCLS	2.5–16.9	280–12,800	120	5–400
SACLA	5.1–8.5	4,000–20,000	60	2–10
FERMI	1–1.5	20–310	50	30–100
PAL-XFEL	3.5–10	275–20,000	60	5–100
SwissFEL	2.1–5.8	250–1,240	100	1–20
European XFEL	8.5–17.5	240–25,000	2.7×10^4	3–150
SXFEL	1.0–1.6	124–1,000	50	30–1,000
LCLS-II (HE)	4–15	200–25,000	$120/10^6$	1–500
SHINE	8	400–25,000	10^6	3–600

Note that only a portion of their performance is listed here for indication. In addition, the pulse duration varies with the operating mode of the facility, such as low charge and two-color mode. More detailed information can be found on their websites.

and a 30th EEHG setup have been demonstrated. In the user phase, the electron beam will be boosted to 1.5 GeV, meaning that the FEL wavelength will cover the water window region.[24] To fulfill the scientific requirements of different research fields, the electron beam will be switched to two undulator arrays, i.e., one seeding line and one SASE line. In the seeding undulator line, there is a plan to deliver a 3–10 nm FEL output with a peak power of a few hundred megawatts, ~50 fs pulse duration, and polarization control feature. The SASE undulator line is based on in-vacuum planar-type undulators with a period of 16 mm. Its final FEL output wavelength ranges from approximately 2–7 nm, with the pulse energy at 2 nm approximately 100 μJ corresponding to a pulse length of approximately 200 fs. The combination of the seeded and SASE undulator lines enables all output properties of the FEL to be controlled, including the central wavelength, bandwidth, pulse duration, polarization, synchronization, longitudinal phase, and implementation of multi-color operation in the near future. Five end stations, including cell imaging, atomic, molecular, and optical science, ultrafast physics, and surface chemistry, were initiated at the beginning of user operation. A more detailed description of the scientific applications supported by the excellent properties of SXFEL can be found elsewhere.[24]

Superconducting linac-based XFEL facilities

Another branch of XFEL evolution over the past two decades concerns the average power capabilities of XFEL facilities, which has been facilitated by the development of high repetition rate electron beam sources in superconducting radio frequency (RF) linear accelerators. Such XFEL sources offer ultrabright, fully coherent, femtosecond X-ray pulses with megahertz repetition rates over a broad photon energy range. In addition, more scientific instruments can be operated in parallel because of the high repetition rate feature.

The development of high repetition rate XFELs was aided tremendously by the pioneering work on FELs at FLASH in Hamburg, which is the world's first soft X-ray FEL user facility.[18] Until successful lasing was demonstrated at LCLS, FLASH was the only short-wavelength FEL user facility worldwide; therefore, all the scientific experiments performed at FLASH were new and unique. Starting user operations in 2005, FLASH not only paved the way for many new FEL developments, but also spearheaded the development of FEL applications in diverse scientific fields.[88] In FLASH, a 1.25 GeV electron beam with a peak current of 2 kA and a micro-pulse repetition rate up to 4.5 MHz is generated by a superconducting linear accelerator. Two undulator lines (FLASH1 and FLASH2) are located downstream, simultaneously providing X-ray laser beams with large independent photon beam parameters. FLASH1 supports five experimental stations with a tunable wavelength range from 4.2 to 52 nm, including stations designed for electron and ion imaging spectroscopy, THz–XUV pump-probe experiments, and time-resolved resonant X-ray scattering experiments. FLASH2 provides a 4–90 nm FEL output to six further experimental stations.

Further to generating FELs for users and developing accelerator technologies, FLASH also serves as a prototype for the European XFEL.[26] The European XFEL started user operation in summer 2017 and is the biggest X-ray laser in the world. The European XFEL is capable of producing 27,000 XFEL pulses per second with 10 Hz macro-pulses that include 2,700 individual pulses, each separated by 220 ns, and a maximum feasible repetition rate of 5 MHz. The electron beam energy can be varied from 8 to 17.5 GeV, while the bunch charge can also be changed from 20 to 1,000 pC, with the bunch length changing from 3 to 150 fs full width at half maximum (FWHM). Owing to the use of variable-gap undulators, photon energies from 0.25 to 25 keV can be achieved at the European XFEL. Five undulator lines in separate parallel tunnels are located downstream of the accelerator, while a sophisticated distribution system is utilized to distribute the electron bunches into each undulator beamline individually, thus enabling the simultaneous operation of multi-experiment stations. At present, three undulator beamlines are available at the European XFEL. Two of these, SASE1 and SASE2, provide 0.4–0.05 nm FEL radiation to four end stations: single particles, clusters and biomolecules, and SFX X-ray experiments at SASE1; materials imaging and dynamics, and high-energy density experiments at SASE2. In contrast, SASE3 has a tunable wavelength range from 4.7 to 0.4 nm, and serves small quantum systems, spectroscopy, and coherent scattering stations.

In light of the obvious improvements to the average brilliance at superconducting facilities and the qualitative change of FEL applications in diverse scientific fields, SLAC also commenced an upgrade project (LCLS-II) in 2014. Here, a 4 GeV superconducting linac generates soft X-ray FEL pulses with a repetition rate up to approximately 1 MHz with an even pulse separation.[25] In 2017, an 8 GeV high repetition rate XFEL facility based on a continuous-wave (CW) superconducting RF Linac was proposed in China, named SHINE.[27] SHINE is the first hard X-ray FEL in China, and aims to generate coherent FEL radiation from 0.4 to 25 keV. At a similar time, LCLS-II announced its high-energy upgrade (the LCLS-II-HE), which increased the beam energy to 8 GeV and the photon spectral range to 12.8 keV. In addition, a modification to the electron injector and beam transport extended the available wavelength range to over 20 keV.

LCLS-II is located within the original 2-mile-long linear accelerator tunnel at SLAC, and has a total length of 600 m. Two adjustable-gap undulator beamlines are located downstream of the accelerator to generate coherent XFEL radiation, with the soft X-ray undulator covering energies from 0.2 to 1.3 keV, and the hard X-ray undulator covering energies from 1 to 5 keV. To meet the scientific requirements for precision measurements of the structural dynamics at atomic spatial scales and fundamental timescales, LCLS-II has been designed to extend the FEL tuning range to the hard X-ray regime, which has been used for more than 75% of LCLS experiments. The extension of the tunable FEL wavelength range is facilitated primarily by the increase of the beam energy from 4.0 to 8.0 GeV. Further to the end stations at LCLS, three new instruments are planned for LCLS-II. First, a time-resolved atomic, molecular, and optical science station that takes full advantage of the 0.25–2 keV energy range provided by LCLS and LCLS-II. Second, a station dedicated to X-ray pump and X-ray probe techniques for conducting "tender" X-ray spectroscopy measurements and serves as a coherent scattering/forward diffraction instrument for sub-micron samples covering the tender X-ray range. At the third station, fully coherent X-rays will be delivered in a uniformly spaced series of pulses with a programmable repetition rate and rapidly tunable photon energies to capture rare chemical events, characterize fluctuating heterogeneous complexes, and reveal quantum phenomena in matter.

SHINE is the most recently proposed high repetition rate hard X-ray FEL facility, and is based on an 8 GeV superconducting accelerator. As shown in Figure 6, it is located at Zhangjiang Scientific City.[27] The whole facility is constructed ~30 m underground and has a total length of 3.1 km, spanning

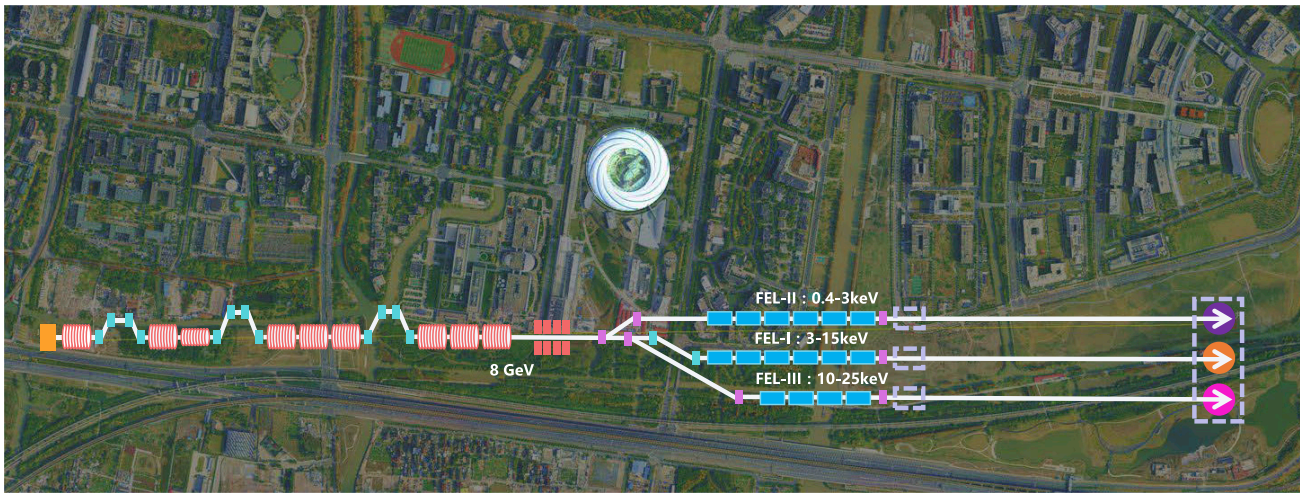

Figure 6. Machine layout of the SHINE facility at Zhangjiang, Shanghai.

the Shanghai Synchrotron Radiation Facility and SXFEL campuses. The machine layout of the SHINE facility is shown in the bottom panel of Figure 6. A 1 MHz electron beam is generated in a VHF photocathode gun and accelerated to ~100 MeV. Next, the beam is accelerated to 8 GeV in the main accelerator and compressed to 1.5 kA longitudinally via two bunch compressors working at energies of 270 MeV and 2.1 GeV, respectively. The 8 GeV electron beam is switched to three undulator beamlines by the beam distribution system. The FEL-I and FEL-II beamlines are based on out-vacuum planar, hybrid permanent-magnet-type undulators to generate FEL radiation from 3 to 15 keV and 0.4–3 keV, respectively. In contrast, FEL-III utilizes the superconducting undulator, yielding photons with energies ranging from 10 to 25 keV. Moreover, each FEL line is equipped with a self-seeding scheme, while EEHG-HGHG cascading is adopted for FEL-II, which will test unprecedented harmonic numbers, such as the 200th harmonic. The initial phase of SHINE involves ten end stations, including CDI, time-resolved photoelectron spectroscopy/microscopy, ultrafast X-ray absorption/emission scattering spectroscopy, SFX, and the extreme light station, among others. Note that tunnel space is reserved for developing three further undulator lines in future, providing SHINE with the potential for XFEL expansion.

More recently, a high repetition rate soft X-ray FEL facility is proposed in Shenzhen, China. A superconducting linac will be built to deliver 2.5 GeV high-brightness electron beams at 1 MHz. With four undulator lines, it will cover the entire soft X-ray spectral range.

CURRENT AND FUTURE APPLICATIONS OF XFELs

XFELs extend the application of lasers to the X-ray regime, using which elemental and chemical state specificities can be studied by exciting and probing core-level electronic transitions. By taking advantage of the ultrashort pulse duration properties of XFELs, time-resolved measurements of molecular dynamics can be performed at natural atomic timescales. Owing to their unprecedented high brightness, XFELs also induce nonlinear X-ray interactions with matter and allow material exploration under extreme conditions. Furthermore, ultra-intense highly coherent hard XFEL pulses have great potential for single-particle scattering imaging of protein molecules without crystallization.

Ultra-short pulse duration applications

The typical time duration of an XFEL pulse is roughly three orders of magnitude shorter than a typical pulse from a synchrotron-derived light source. As their pulse lengths are typically shorter than 100 fs down to a few femtoseconds, XFEL pulses enable simultaneous high spatial and temporal resolution that was previously unattainable. Many of the fundamental chemical interactions in matter happen over timescales spanning a few tens of femtoseconds. In addition, phenomena, such as vibrational dynamics and bond-breaking exhibit timescales ranging from 10 fs to 1 ps. Therefore, XFELs are ideal tools to study these interactions. Such time-resolved experiments mainly utilize pump-probe methods. Pump-probe schemes utilize two light pulses, with one pulse interacting with the sample to initiate the dynamics, while the other provides observables to monitor the response. The temporal resolution is determined by the combination of the pulse duration and the delay control between the pump and probe pulses.

As demonstrated by LCLS in recent years, XFELs facilitate high-temporal-resolution pump-probe experiments using X-ray pulses. The transient states and molecular dynamics induced by optical pump pulses can be detected by an X-ray probe pulse through non-resonant scattering and spectroscopy. Molecules undergo ultrafast charge density redistributions when interacting with electromagnetic fields and the resulting photoexcitation is the first step in all photochemical and photophysical processes. For example, gas-phase time-resolved X-ray scattering has been used recently to observe the molecular electronic response of 1,3-cyclohexadiene to UV light upon photoexcitation.[89] Furthermore, as shown in Figure 7, soft X-ray spectroscopy has been used to reveal the dynamics of the valence holes created by 800 nm strong-field ionization in water and track the primary photon transfer reaction.[90]

The rapid development of XFEL has led to two-color X-ray pulses with a tunable delay, thus opening new opportunities for X-ray pumps and X-ray probes, which can be used for studying the ultrafast dissociation and charge migration induced by X-rays. Because X-rays interact predominantly with inner-shell electrons, they excite a specific site or atomic species. Therefore, by tuning the incident photon energy, photoabsorption can be controlled and localized at specific sites within large molecules. The charge migration and charge transfer that follow core-excitation occurat timescales ranging from sub-femtosecond to a few femtoseconds, and are essential for chemical reactions. The charge redistribution and Auger cascades from biological objects containing, for example, sulfur, selenium, and iodine atoms, can be observed using X-ray diffraction and have attracted considerable attention.[91,92] Moreover, ultra-short coherent pulses serve not only for observing the fast motion of electrons, but also provide the tools to manipulate electron dynamics and control matter in unprecedented ways. The ultra-short pulses create coherent electronic excitations, thereby showing excellent prospects for developing coherent quantum control methods.

Ultra-short (i.e., femtosecond) X-ray pulses are used in single-shot images, which can generate diffraction signals before destruction.[93] One key challenge facing XFEL single molecular high-resolution imaging is the radiation damage induced by X-ray photoionization and Auger decay. The ions created by X-ray photons repel each other, and the ultrafast electrodynamics of the target molecule within the XFEL pulse duration degrade the scattering pattern. These electronic damages happen at timescales ranging from hundreds of attoseconds to a few femtoseconds. To avoid these damages

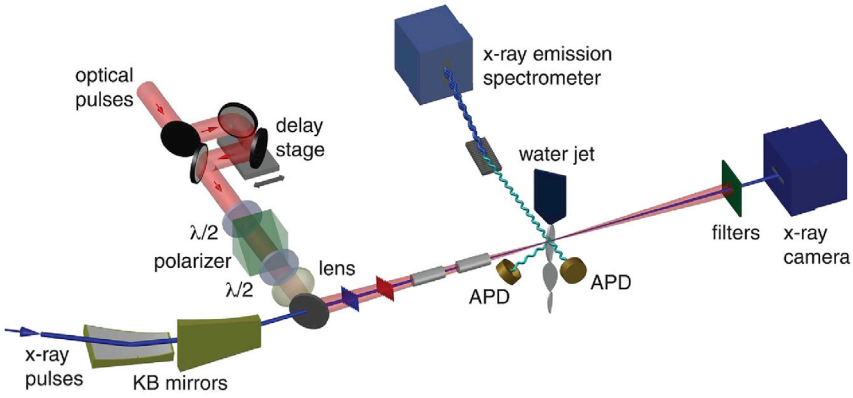

Figure 7. Schematic of laser pump X-ray probe experiments Water in the jet is ionized by a strong field at a wavelength of 800 nm, with the fluorescence and transmission spectra measured after the time-delayed X-ray probe pulse to reveal the fast-chemical processes that occur in the radiolysis of water. From Loh et al.[90] Reprinted with permission from AAAS.

having an impact on the imaging, ultra-short X-ray pulses are required to produce diffraction signals before the change of molecular geometry. Recent theoretical simulations suggest that the creation of hollow-atoms in carbon via ultrafast high-intensity XFEL pulses is feasible. X-ray scattering saturation occurs at a flux intensity of $\sim 10^7$ photon/Å^2 and the frustrated absorption of ultra-short X-ray pulses reduces the radiation damage.[94] With the advent of high repetition rate XFELs, novel methods, such as ghost imaging and X-ray fluorescence imaging, are considered possible and are under development.

High peak intensity applications

The emergence of short-wavelength FELs, which deliver ultra-intense X-ray pulses that exceed the peak brilliance of synchrotron light sources by 10 orders of magnitude, opens a pathway for studying the nonlinear interactions of X-rays with atoms and molecules. Multiphoton physics in an X-ray regime differs considerably from long-wavelength regimes, for which photons do not carry sufficient energy to ionize atoms and the most common interactions are multiphoton ionization or quantum tunneling ionization. Owing to their high photon energy, X-rays can ionize atoms via single photon absorption. The dominant channel of interaction is multiphoton sequential ionization, whereby atoms absorb more than one photon via a single X-ray pulse. The combination of sequential photoionization with Auger decay forms highly charged atomic states, which cannot normally be achieved using traditional low-fluence X-ray sources. For pulse durations shorter than the Auger decay time (a few femtoseconds), the photons at the end of an XFEL pulse encounter atoms in different states. The inner-shell vacancies produced by photons at the beginning of the process suppress photoabsorption and lead to intensity-induced X-ray transparency.[95] More efficient photon absorption occurs for molecules containing heavy atoms, in which the ultrafast charge redistribution from neighboring atoms refills the core-holes before Auger decay occurs.[92] Note that the X-ray analogy of high-order nonlinear optical processes, such as two-photon absorption, competing against single and sequential multiphoton processes, and XFELs, enable the measurement of small cross-sections.[96]

Nonlinear phenomena enabled by intense light sources in the optical, infrared, and microwave regimes have all been utilized to control electronic, nuclear, and spin transitions, leading to breakthroughs in multiple scientific fields, such as medical imaging, telecommunications, and the creation and manipulation of novel materials. Exploring nonlinear light-matter interactions in the X-ray regime invites the possibility of transferring these techniques to the X-ray domain, thereby creating opportunities to elucidate material dynamics at more suitable energies and spatial resolutions. Mixing X-rays and optical waves facilitates the direct observation of microscopic fields in materials via optical lasers.[97] Nonlinear spectroscopies, such as stimulated electronic X-ray Raman scattering, enable interesting phenomena, including the coherent interplay of electronic and vibrational degrees of freedom, energy transfer in light-harvesting complexes, and reaction dynamics of catalytic processes, to be studied.[98] Moreover, through pumping XFELs with dense gases, population inversion is created via inner-shell photoionization. Thus, atomic inner-shell X-ray lasers with higher wavelength stability, monochromaticity, and improved temporal coherence are generated at the end of the excited plasma.[99]

Applications using coherence

CDI is a lensless imaging method that records the diffraction patterns resulting from interactions between incident coherent X-rays and samples, before phasing the diffraction patterns using a phase-retrieval algorithm.[100] The significantly improved coherence and brightness of XFELs relative to synchrotron radiation, make XFELs ideal tools for CDI. Several new CDI-based techniques have been developed for both static and time-resolved diffraction studies of biological macromolecules, in particular SFX and single-particle imaging (SPI). By utilizing the unique properties of XFELs, these techniques expand the capabilities of CDI to difficult-to-grow targets, such as nanocrystals, which is important because many samples in physics, chemistry, materials science, nanoscience, geology, and biology are non-crystalline; therefore, their 3D structures are not accessible by traditional X-ray crystallography.

The first high-resolution SFX results were obtained at LCLS in 2011.[101] The experiments were performed at coherent X-ray imaging beamlines using X-rays with an energy of 9.4 keV (a wavelength of 1.33 Å) with a 40 fs pulse duration and an average pulse energy at the sample of 600 μJ per pulse. Statistical data were obtained with a resolution of 1.9 Å. The experiments also show that structures that are typically too small to be used for synchrotron-based crystallography can be characterized at near atomic resolution using SFX without significant destruction at room temperature. Furthermore, time-resolved SFX with resolution of 1.6 Å allows determination of the structures of reaction intermediates.[102] Overall, SFX with XFELs creates new opportunities to extract structural information from thousands of nanocrystals that are too small to be determined using synchrotron radiation, and promises to accelerate progress in overcoming challenging problems in structural biology.

For SPI, the ultimate goal is to reveal the dynamic structure of single particles or macromolecules (without requiring crystallization) at room temperature with atomic-scale resolution.[103] Figure 8 shows the first SPI results acquired for biological samples at LCLS.[104] High-quality diffraction data were obtained from a mimivirus using a single X-ray laser pulse. The reconstructed image shows a full-period resolution of 32 nm. However, the challenges of reaching sub-nanometer resolution with SPI are immense. Because even viruses as large as the mimivirus (approximately 0.3 μm in diameter) scatter only a few million soft X-rays when hit with XFEL pulses, obtaining complete diffraction patterns of single particles is difficult. As a consequence, in such experiments, components, including the sample delivery system, the high-precision X-ray mirrors, the high-sensitivity X-ray detector, and the phasing algorithm, must be optimized.[103] The achievable resolution has increased from more than 100 nm to less than 10 nm today.[105,106] For further resolution improvements, more intense XFEL pulses as well as thousands of diffraction patterns from equivalent samples are required.[107] Thus, high repetition rate

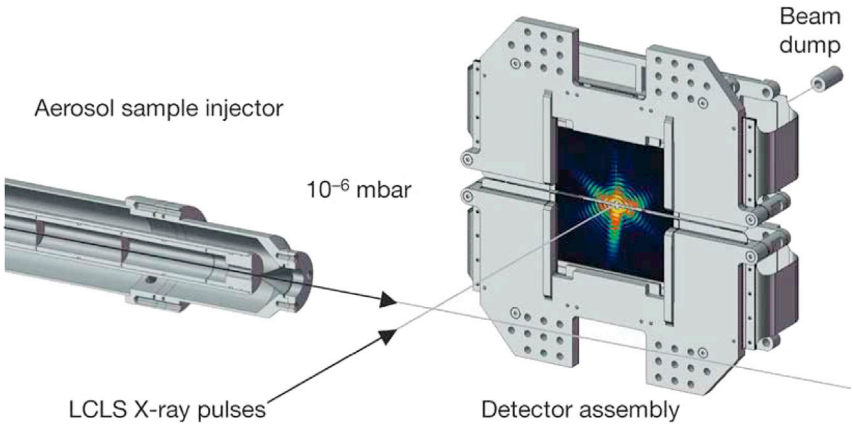

Figure 8. Schematic of the experimental arrangement for imaging single virus particles at LCLS The experiment results show that one can obtain a clearly symmetrical diffraction pattern of a non-crystalline giant mimivirus particle using a single LCLS pulse. Reprinted with permission from the Copyright Clearance Center: Springer Nature, Nature (Seibert et al.[104] Single mimivirus particles intercepted and imaged with an X-ray laser), Copyright (2011).

XFELs, such as the European XFEL, LCLS-II, and SHINE, are promising light sources for high-resolution SPI.

In addition, using the "diffraction-before-destruction" mode, the femtosecond pulses of the XFEL can outrun most radiation damage processes. Furthermore, this mode allows proteins to be studied at room temperature rather than the low temperatures used at synchrotrons to minimize radiation damage. Therefore, XFELs provide an important opportunity to study time-resolved protein dynamics at room temperature provided that the correct physiological driving forces and energies are available. For the first time, true nanoscale structures of living cells can be imaged using X-rays.[108,109] Moreover, by obtaining diffraction patterns with single XFEL pulses, it is possible to study dynamic processes at a femtosecond timescale and an atomic-level spatial scale. In addition, when combined with pump lasers, SPI becomes an important tool for elucidating dynamic processes in materials science, such as phase transitions and melting processes at a picosecond timescale and a nanoscale spatial scale.[110,111]

XFELs and extremely intense lasers

New possibilities arise when combining an XFEL with high-power optical lasers. Laser pulses with a peak power of 10 PW (peak intensities beyond 10^{22}W/cm^2) are close to being achieved in several ongoing projects, such as ELI,[112] Apollon,[113] Vulcan,[114] and SULF,[115] providing a powerful approach for studying material properties under extreme pressure, lab astrophysics, and nuclear physics. Highly coherent short-wavelength XFELs are an excellent probe for mapping the dynamics of these microscopic processes during laser-matter interactions. Moreover, quantum electrodynamics predicts that vacuums can be polarized by ultra-strong laser fields.[116] The subtle difference between the refractive indices along the electric and magnetic fields in a vacuum leads to a birefringence effect for light propagating through the vacuum. This effect, known as vacuum birefringence, has never been observed in the laboratory. By colliding an XFEL beam with a high-power laser, the purely linearly polarized X-ray photon beam is predicted to be modified, becoming elliptically polarized.[117] For example, in the "Station of Extreme Light (SEL)" at SHINE, a 100 PW laser is being built to perform head-on collisions with the 3–15 keV XFEL beam,[118] with the aim of detecting the X-ray ellipticity from vacuum birefringence. X-ray beam ellipticity in the range of 10^{-10}–10^{-9} is expected, which is close to the threshold of current polarity detection techniques.[119]

CURRENT DEVELOPMENTS AND FUTURE PROSPECTS FOR XFELs

Over the past 10 years, the applications involving XFELs have undergone rapid and important advances. Unprecedented development of FEL facilities and the corresponding experimental technologies are driven by huge demand from scientific user communities. This mutually reinforcing relationship has heralded a golden age of development for FEL facilities in the past two decades. Following the requirements from the user communities, current directions of FEL development are aimed toward the generation of transform-limited FEL pulses, the reduction of pulse lengths below the electron bunch length (that is, the attosecond regime), the increase of output power beyond the normal saturation level (that is, toward terawatt FELs), the generation of high repetition rate XFEL pulses, and the reduction of the size of XFEL facilities. In this section, we briefly discuss novel developments in these areas.

Precise pulse control

One-revolution XFELs have brought to the field of ultrafast X-ray spectroscopy is the ability to generate ultra-short, high-brightness X-ray pulses. To shorten the pulse duration, it is necessary to generate a shorter electron beam or shape the electron beam itself so that only a small part of the electron beam is used for lasing in the FEL. With the help of an emittance spoiler or low-charge operation, the XFEL pulse duration can be depressed to an FWHM of approximately 5 fs.[120,121] To generate sub-femtosecond X-ray FEL pulses, an enhanced SASE (ESASE) approach has been proposed, with the idea of compressing parts of an electron bunch via an external infrared laser.[122] To reduce the peak power requirement of the external laser system, angular dispersion ESASE has been proposed.[123] Transverse-longitudinal phase space coupling is introduced via the energy modulation and momentum compaction, which can decrease the peak power requirement by more than an order of magnitude. Recently, a scheme that involves coherent infrared radiation emitted by the tail of the electron beam in a wiggler, rather than an external infrared laser, to manipulate the electron beam in the ESASE mode was proposed and demonstrated experimentally in two separate studies.[124,125] The experimental data show that the X-ray laser-enhanced attosecond pulse (XLEAP) generation setup is capable of producing a median duration of 280 attoseconds (FWHM) at 905 eV,[125] as shown in Figure 9. In addition, utilizing the energy chirp of the electron beam in combination with an optimized undulator tapering, attosecond XFEL pulses can be obtained as only a small part of electron beam can satisfy the resonance condition of FEL lasing.[126]

Another aim of the next stage of XFEL developments will increase the peak power to the terawatt level. In addition to generating attosecond pulses, the ESASE scheme is best positioned to generate terawatt FEL pulses,[127,128] as part of the electron beam is compressed into a high localized peak current. Another promising approach for reaching terawatt powers with very high pulse energies is to increase the electron-radiation energy transfer efficiency. To achieve this, a tapered undulator, in which the magnetic field varies along the undulator length, has been proposed, with this technique allowing the undulator to be adjusted to satisfy the resonance condition via electrons that have lost energy for further energy extraction. This has been studied theoretically via numerical simulations,[129,130] and demonstrated experimentally at microwave wavelengths. Several recent studies have used model-based methods in conjunction with an evolution algorithm to find the optimal tapering laws.[131]

In recent years, the use of two-color X-ray pulses for ultrafast pump-probe experiments has been the subject of intense investigation. Two-color FELs

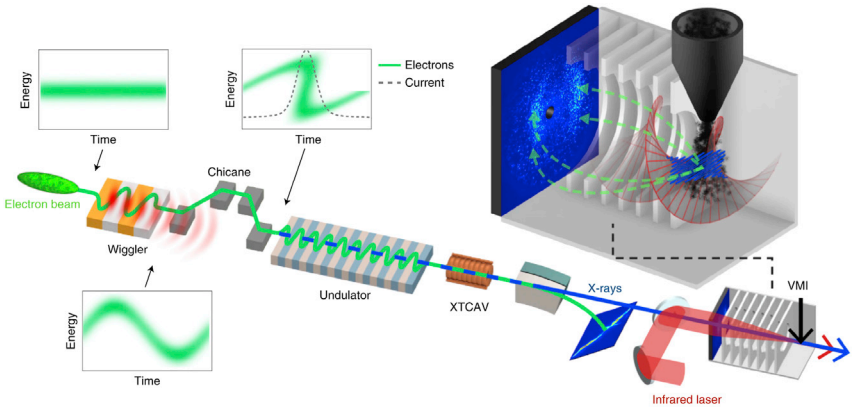

Figure 9. Illustration of XLEAP operation The electron beam forms a single-cycle energy modulation by itself in a long-period wiggler. Then, the energy modulation is transferred into a single density spike for generating attosecond X-ray pulses. This setup is naturally compatible with high repetition rate XFELs, as it is based solely on a passive wiggler. Reprinted with permission from.[125] Reprinted with permission from the Copyright Clearance Center: Springer Nature, Nature Photonics, (Duris et al.,[125] Tunable isolated attosecond X-ray pulses with gigawatt peak power from a free-electron laser), Copyright (2020).

can generate two X-ray pulses with different photon energies and a variable delay. The two-color FEL schemes that have been developed and tested thus far can be divided into two main categories: twin-bunch FELs,[132] for which different beam energies are used to make pulses of different colors, and two undulator schemes,[133–135] in which undulators with different magnetic fields are obtained by dividing the undulator system into two sections longitudinally, with a distinct *K* value associated with each section. Results from LCLS show that the time delay between two FEL pulses can be adjusted within 100 fs, and the peak-to-peak spectrum separation is approximately 90 eV at 8.3 keV.[133] Another method of generating two or more spectral lines involves a gain-modulated FEL, which uses a periodic modulation of the undulator parameter. The periodicity controls the number of colors and the gain per color.[134] A further alternative approach, called "fresh-slice," allows only a fraction of the electron bunch to lase in each undulator, thereby allowing the FEL to reach different colors.[136] In hard X-ray self-seeding setups, two-color FEL pulses can be generated by rotating the self-seeding crystal to transmit two narrow-width colors that are both amplified by the same electron bunch.[137]

Further research has focused on methods for obtaining tunable polarization in XFELs. Several schemes have been developed for this purpose, including crossed-planar undulators[138,139] and elliptical permanent undulators in after-burner.[140,141] The crossed-planar undulator consists of horizontally and vertically polarized undulators with a phase shifter inserted between them. This structure enables flexible polarization switching at a high rate. The drawback of this scheme is the relatively low degree of polarization because the two linearly polarized lasers are emitted separately at two undulators, with the superposition of the two polarized beams requiring high coherence. In contrast, the elliptical undulator can produce highly polarized FEL pulses consistently and has been implemented in several facilities. A typical example is the Delta undulator, which has been installed at LCLS. Experiments at LCLS show that radiation from the Delta undulator exhibits an extremely high degree of circular polarization relative to crossed-planar undulators. However, switching the polarization at kilohertz rates by adjusting the Delta undulator mechanically is challenging.

High repetition rate XFELs

High repetition rate XFELs based on superconducting linacs have been proposed to obtain high average brightness, which is useful for many scientific applications. The European XFEL can provide 27,000 pulses per second using its pulsed mode. Based on a CW superconducting linac, LCLS-II and SHINE are both capable of providing FEL pulses with repetition rates up to 1 MHz. Following the rapid development of high repetition rate XFELs, several of the previously mentioned XFEL schemes have been adapted for high repetition rates, especially with respect to the heat load effect caused by high repetition. Furthermore, many fundamental experiments are being developed to take advantage of high repetition rates. For example, high repetition rate instruments have the potential to reduce the time required to perform X-ray spectroscopy and solution-scattering experiments from hours to a few seconds, leading to huge enhancements in data quality and quantity; additionally, they would allow us to measure more time points in time-resolved experiments involving single crystals and solution scattering. In addition, high repetition rates enable us to capture a high number of images for single-particle diffraction, which may increase the resolution limit significantly.

One advantage of high repetition rate XFELs is that they can provide more experimental stations through the parallel operation of multiple undulator lines. However, the simultaneous operation of these undulator lines requires a large and adjustable spectrum. Usually, the tunable range of the spectrum is limited by the tunable range of the undulator magnetic field strength. In addition, a large adjustable range of photon energies is needed to change the electron beam energy. Two methods have been proposed to tune the beam energy in a single undulator independently. The first is to send the low-energy beam to a specific undulator line via an additional beam spread line.[22] This method is widespread in XFEL facilities but offers limited adjustability. The second method provides bunch-to-bunch energy-changed electron beams at the end of the linac by changing the specific RF units at the subharmonics of the trigger frequency.[142] Not all electron beams are accelerated when passing through these RF units, which means lower energy beams are obtained at the end of the linac. This scheme can obtain electron beams with large energy differences; however, it is not suitable for machines operated in the high repetition rate mode. Therefore, new schemes have been developed to control the electron beam energy in high repetition rate XFELs with greater precision. A new beam delay system design has been proposed to realize multi-beam-energy operation at SHINE,[143] as shown in Figure 10. This delay system is designed to be achromatic and isochronous and is placed before the last accelerating section. Consequently, the arrival time of the electron beam at the last accelerating section is changed, which means a different accelerating phase. Combined with fast kickers, such a system can be used to generate bunch-to-bunch energy-changed beams in high repetition rate XFELs. In addition, another method that utilizes the off-frequency detune method in superconducting linacs has been proposed to control the energy of multiple electron bunches in high repetition rate XFELs.[144] In this scheme, the resonant frequency of the superconducting cavity is tuned by a frequency tuner, thereby changing the accelerating phase. By detuning different cavities systematically, bunch-to-bunch energy-changed electron beams can be obtained.

In addition to controlling the energy of electron beams, the longitudinal phase space manipulation of electron beams is also critical for several advanced FEL schemes. As mentioned earlier, seeded FELs rely on the energy modulation of an external seed laser. However, because of the limitations of state-of-the-art laser systems, it is difficult to operate seeded FELs at a high repetition rate. Therefore, more advanced laser systems, such as the optical parametric chirped-pulse amplification (OPCPA) technique, are under development. Using the OPCPA technique, a repetition rate of up to 100 kHz can be achieved. In addition to developing the external laser system, methods that use cavity-based FELs as a seeding source are also proposed. Extreme UV FEL oscillators driven by 2–2.6 GeV electron beams have been

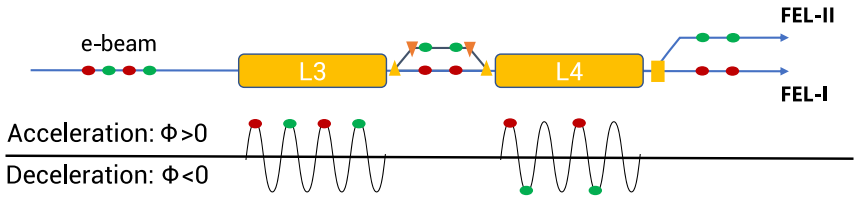

Figure 10. Schematic layout of the electron beam delay system for CW-linac-based XFELs

proposed as a seeding source for a triple cascade, thereby generating few Ångstrom-class radiation.[145] As the energy spread is large when the FEL oscillator is saturated, multi-bunch operation is needed for this scheme to achieve a high peak power. Recently, a resonator-like seed recirculation feedback system was proposed in which the radiation in the cavity is recirculated to modulate following bunches but is far from saturation.[78] Furthermore, a self-modulation method has been proposed recently for enhancing laser-induced energy modulation, which significantly reduces the requirement for an external laser system. Using this scheme, an HGHG FEL that uses an energy modulation as small as 1.8 times the slice energy spread has been demonstrated.[146]

Combining FELs with storage rings

Storage ring (SR)-based light sources are a mature and reliable method for delivering EUV and X-ray radiation pulses with high stability and high repetition rates via multiple beamlines simultaneously. SR-based synchrotron radiation sources, which first appeared in the 1960s, have undergone three generations of development and evolution, and are currently moving toward the fourth generation, which aims to deliver diffraction-limited SRs with higher brightness and better transverse coherence.[3,4] Over the last decades, evolutionary increases in the brightness of SR sources have birthed a robust array of X-ray capabilities. Although the SR-based synchrotron radiation with pulse durations as short as a few tens of picoseconds have become a standard tool for studying the structure of matter on the atomic scale, their pulse durations are still too long to measure atomic motion and structural dynamics at the fundamental timescale of a vibrational period. In addition, synchrotron radiation pulses are not suitable for certain high-resolution spectroscopy and imaging experiments because of the low peak power and incoherent in time. The urgent need for intense ultra-short radiation pulses has prompted further FEL developments. While, at present, there are 8 short-wavelength FEL facilities serving as single or multi-user facilities worldwide, while there are over 50 synchrotron light sources routinely providing X-rays to multiple users simultaneously. The emergence of combined SR and FEL concepts for the construction of ultra-short high-intensity coherent light sources has attracted significant attention from the accelerator and light source user communities.

The main purpose of combining FELs and SRs is the generation of coherent ultra-short pulses in existing synchrotron radiation sources. Although various schemes have been developed in recent decades, only few of them seem to be compatible with the preservation of high intensity. Although, the SASE principle has been considered for SRs[147–149], the SASE mechanism typically requires a relatively long undulator (~ 100 m) to amplify the initial emission from electron beam noise; thus, the capacity of SR-based SASE is undoubtedly limited. Furthermore, a beam energy spread of 1%, which significantly exceeds the typical FEL gain bandwidth of ~ 0.1%, is expected in SR undulators. Further, SR-FELs based on TGUs have been proposed[150] to overcome the energy spread mismatch. However, this approach brings new challenges concerning the control of the electron beam envelope while considering the strong quadrupole field of the TGU.

An alternative method for combining the coherent micro-bunching of FELs with SRs is to use external lasers to optically manipulate and pre-bunch the electron beam at the optical scale. Coherent harmonic generation (CHG)[29] or optical klystron[151] is the most representative pre-bunching mechanism and has been applied successfully to SRs to generate ultra-short coherent pulses. Generating micro-bunching at the *n*th harmonic of the seed laser requires the energy modulation amplitude to be approximately *n* times larger than the initial beam energy spread. Because of the large inherent energy spread of the electron beam in SRs, the harmonic number of standard CHG is approximately one order of magnitude lower than what is required for reaching the EUV and soft X-ray regions. To enhance the harmonic multiplication efficiency, EEHG has been proposed for manipulating the electron beam phase space in SRs.[152,153] However, the laser-induced energy spread remains too large for short-wavelength generation. Using the PEHG scheme with a TGU as the modulator has also been proposed for improving the performance of CHG,[56] and it was later found that the bunching of the PEHG decreases significantly for very small energy modulations due to transverse phase space coupling during pre-bunched electron beam preparation.[58] The harmonic up-conversion efficiency can also be enhanced by tailoring the angular divergence of the electron beam instead of the energy spread. A laser operating in the TEM_{01} mode has been proposed for modulating the angular distribution of the electron beam in the modulator.[154] After passing through a beamline designed with a non-zero value for transfer matrix element R_{54}, the angular modulation is converted to a density modulation that contains the high harmonic components of the seed. Although the balance between quantum excitation and radiation damping in the SR results in a relatively large energy spread, it also provides a beam with very low angular divergence. The proposed scheme makes full use of this characteristic to obtain much higher harmonic numbers. One drawback of this method is the requirements of complex lattice structures and lasers with a peak power measuring hundreds of gigawatts. In addition, several methods with angular dispersion elements or an obliquely incident laser have been developed[155–157] to effectively tailor the electron beam angular divergence for CHG, resulting in an angular divergence of~10 nm being achieved. The advantage of these methods is that the required energy modulation amplitudes can be much smaller than the electron beam energy spread. As a result, megawatt lasers provide sufficient power, thereby allowing lasers with much higher repetition rates than conventional CHG to be used. Together with the very small correlated energy spread promised by these schemes, the higher extent of bunching significantly increases the number of coherent photons per pulse and relaxes the constraints on the SR operation. Nevertheless, concerns about the SR lattice design remain, especially with respect to the long drift section and emittance degradation due to the angular divergence manipulation and shorter wavelength extensions.

In addition, the steady-state micro-bunching (SSMB) mechanism has been proposed to utilize micro-bunching in electron SRs.[158–160] The idea of SSMB is to manipulate the particle dynamics in a dedicated lattice, usually using laser modulators as the bunching systems. This induces micro-bunching, which is sustained in a turn-by-turn steady state each time the beam passes through the radiator. By combining the micro-bunching-enabled coherent emission with the near-light-speed revolution of particles in an SR, SSMB promises high-power radiation with a high repetition rate (MHz to CW) and a narrow linewidth at wavelengths ranging from the terahertz to the EUV regions. These novel photon sources are expected to provide unprecedented opportunities for scientific and industrial applications. For example, SSMB is one of the most promising schemes for generating high-power EUV radiation, which is urgently needed for lithography in semiconductor technologies. A task force has been established at Tsinghua University, with a collaboration comprising researchers from China, Germany, the USA, and elsewhere, assembled to promote SSMB research and to develop an SSMB SR. Active research concerning SSMB-related physics and technology is ongoing.[159,160] Recently, the SSMB mechanism was demonstrated

experimentally for the first time by the Tsinghua University collaboration at the Metrology Light Source.[160]

Progress toward ultra-compact XFELs

The success of XFELs is strictly related to the generation of high-brightness, high-energy electron beams from linear accelerators. However, accelerators equipped with XFELs are based on conventional or superconducting RF accelerating structures, which limit the compactness of the machine. Therefore, XFELs are large facilities, with the smallest approximately 0.7 km in length. Thus, the development of ultra-compact XFELs has focused predominantly on advanced accelerators. Particularly, plasma-based (wakefield) accelerators (PBAs) driven by either charged particle beams (plasma wakefield accelerators) or intense lasers (laser wakefield accelerators), in which a beam is accelerated up to several GeV energies over a very short distance (cm scale), are attractive designs for ultra-compact XFELs. Indeed, recent studies have shown that PBAs with controlled injection schemes have the potential to generate electron beams with energies in the range of several GeV, with a normalized emittance of ~ 10 nm, peak currents of ~10 kA, and normalized brightness of~ 10^{20}A/m^2.[161–164] Such high beam brightness values are far beyond the capabilities of state-of-the-art conventional accelerators; therefore, PBAs promise the realization of compact—with much shorter gain and total undulator lengths—and high-performance FEL light sources that deliver unprecedented brightness. However, the beam divergence (mrad scale) and energy spread (percentage) currently obtained in PBAs are relatively large, thereby preventing straightforward FEL amplification even in the soft X-ray regime.

To build suitable PBA-based XFELs that operate in the soft X-ray regime (i.e., several-nanometer wavelengths), these challenges need to be solved. To tackle beam divergence, plasma matching sections have recently been proposed for transporting the beam from the exit of the PBA (relatively large divergence and small spot size) to the entrance of the undulator (relatively small divergence and large spot size).[165] Three potential solutions have been proposed for minimizing beam energy spread. The first is to utilize a tenuous uniform or hollow channel plasma de-chirper to reduce the beam energy spread.[166–168] This works because, in PBAs, the energy chirp induced by the acceleration phase variance is the dominant part of the total energy spread. The second works on the basis that, because the PBA generated electron beam has a very small emittance, its entire phase space brightness is sufficiently high to drive the XFEL. Thus, in principle, it is only necessary to redistribute the phase space of the laser plasma-accelerated beam to achieve FEL amplification. This occurs via either emittance exchange[169] or longitudinal decompression[170] with chromatic matching. The third possibility is to use a TGU to mitigate the impact of energy spread on the amplification of the FEL.[171,172] These three methods are currently implemented in ongoing PBA-based FEL projects.

SUMMARY AND OUTLOOK

It is clear that XFELs have driven considerable developments in scientific applications and technologies. The purpose of this review is to present a collection of representative samples that highlight the potential of these instruments and to provide references that will assist those who want to learn more.

In terms of FEL applications, there has been huge progress across all fields and further progress is anticipated as FEL technologies continue to mature. For example, ultra-short pulse durations facilitate time-resolved measurements of molecular dynamics at natural atomic timescales. In addition, the unprecedented high brightness of XFELs induces nonlinear X-ray interactions with matter and allows the exploration of materials under extreme conditions. Ultra-intense highly coherent hard XFEL pulses have great potential for single-particle scattering-based imaging of non-crystallized protein molecules. Undoubtedly, as the technology delivering sophisticated photon beams matures (for example, in multi-color pulse generation, fast polarization control, attosecond pulse generation, and pulse shaping) increasingly adventurous experiments will be realized.

In terms of FEL physics, since XFELs first became available to users, many new operating modes have been introduced and tested to meet the requirements of advanced X-ray communities. Most of them have enhanced the output characteristics of light from different aspects and enabled new applications. However, there is still a catalog of creative ideas for manipulating the FEL process further. The aims of these ideas include order of magnitude increases in the output power, pulse duration reduction toward the attosecond scale, control of spectral properties and polarization, the combination of FELs and SRs, and further reduction of X-ray FEL facility sizes. These potential future developments have been discussed to provide a broad picture of the future prospects of XFELs as unique and customizable tools for driving scientific progress.

In terms of FEL facilities, it should be noted that the rapid advancement of FEL applications and technologies has driven increasing worldwide demand for access to XFEL facilities. These facilities are now moving toward high repetition rate operation (up to several MHz) by using superconducting linacs, such as at the European XFEL, LCLS-II, and SHINE. Unsurprisingly, future XFEL facilities will offer a large number of dedicated undulator beamlines that can be optimized for specific types of measurement, thus providing sufficient XFEL time to meet user demand.

REFERENCES

1. Garman, E.F. (2014). Developments in X-ray crystallographic structure determination of biological macromolecules. Science ***343***, 1102–1108, https://doi.org/10.1126/science.1247829.
2. Berman, H.M. (2000). The protein data bank. Nucleic Acids Res. ***28***, 235–242, https://doi.org/10.1093/nar/28.1.235.
3. Zhao, Z.T. (2010). Storage ring light sources. Rev. Accl. Sci. Tech. ***03***, 57–76, https://doi.org/10.1142/S1793626810000361.
4. Hettel, R. (2014). DLSR design and plans: an international overview. J. Synchrotron Radiat. ***21***, 843–855, https://doi.org/10.1107/S1600577514011515.
5. Madey, J.M.J. (1971). Stimulated emission of bremsstrahlung in a periodic magnetic field. J. Appl. Phys. ***42***, 1906–1913, https://doi.org/10.1063/1.1660466.
6. Deacon, D.A.G., Elias, L.R., Madey, J.M.J., Ramian, G.J., Schwettman, H.A., and Smith, T.I. (1977). First operation of a free-electron laser. Phys. Rev. Lett. ***38***, 892–894, https://doi.org/10.1103/PhysRevLett.38.892.
7. Kondratenko, A.M., and Saldin, E.L. (1980). Generating of coherent radiation by a relativistic electron beam in an ondulator. Part. Accel. ***10***, 207–216.
8. Haus, H. (1981). Noise in free-electron laser amplifier. IEEE J. Quan. Electron. ***17***, 1427–1435, https://doi.org/10.1109/JQE.1981.1071289.
9. Derbenev, Y., Kondratenko, A., and Saldin, E. (1982). On the possibility of using a free electron laser for polarization of electrons in storage rings. Nucl. Instr. Methods Phys. Res. ***193***, 415–421, https://doi.org/10.1016/0029-554X(82)90233- 6.
10. Dattoli, G., Marino, A., Renieri, A., et al. (1981). Progress in the Hamiltonian picture of the free-electron laser. IEEE J. Quan. Electron. ***17***, 1371–1387, https://doi.org/10.1109/JQE.1981.1071268.
11. Bonifacio, R., Pellegrini, C., and Narducci, L. (1984). Collective instabilities and high-gain regime in a free electron laser. Opt. Commun. ***50***, 373–378, https://doi.org/10.1016/0030-4018(84)90105-6.
12. Murphy, J.B., and Pellegrini, C. (1985). Generation of high-intensity coherent radiation in the soft-X-ray and vacuum-ultraviolet region. J. Opt. Soc. Am. B ***2***, 259, https://doi.org/10.1364/JOSAB.2.000259.
13. Fraser, J., and Sheffield, R. (1987). High-brightness injectors for RF-driven free-electron lasers. IEEE J. Quan. Electron. ***23***, 1489–1496, https://doi.org/10.1109/JQE.1987.1073544.
14. Pellegrini, C. (1988). Progress toward a soft X-ray FEL. Nucl. Instrum. Methods Phys. Res. A. ***272***, 364–367, https://doi.org/10.1016/0168-9002(88)90252- 5.
15. Carlsten, B. (1989). New photoelectric injector design for the Los Alamos National Laboratory XUV FEL accelerator. Nucl. Instrum. Methods Phys. Res. A. ***285***, 313–319, https://doi.org/10.1016/0168- 9002(89)90472-5.
16. Seeman, J.T., Adolphsen, C., Bane, K.L.F., et al. (1991). Summary of emittance control in the SLC linac. In Conference Record of the 1991, *4* (IEEE Particle Accelerator Conference), pp. 2064–2066.
17. Hogan, M., Pellegrini, C., Rosenzweig, J., Travish, G., Varfolomeev, A., Anderson, S., et al. (1998). Measurements of high gain and intensity fluctuations in a self-amplified, spontaneous-emission free-electron laser. Phys. Rev. Lett. ***80***, 289–292, https://doi.org/10.1103/PhysRevLett.80.289.
18. Ackermann, W., Asova, G., Ayvazyan, V., et al. (2007). Operation of a free-electron laser from the extreme ultraviolet to the water window. Nat. Photon. ***1***, 336–342, https://doi.org/10.1038/nphoton.2007.76.
19. Emma, P., Akre, R., Arthur, J., et al. (2010). First lasing and operation of an Ångstrom-wavelength free-electron laser. Nat. Photon. ***4***, 641–647, https://doi.org/10.1038/nphoton.2010.176.

20. Ishikawa, T., Aoyagi, H., Asaka, T., et al. (2012). A compact X-ray free-electron laser emitting in the sub-Ångström region. Nat. Photon. ***6***, 540–544, https://doi.org/10.1038/nphoton.2012.141.
21. Kang, H.-S., Min, C.-K., Heo, H., et al. (2017). Hard X-ray free-electron laser with femtosecond-scale timing jitter. Nat. Photon. ***11***, 708–713, https://doi.org/10.1038/s41566-017-0029-8.
22. Prat, E., Abela, R., Aiba, M., et al. (2020). A compact and cost-effective hard X-ray free-electron laser driven by a high-brightness and low-energy electron beam. Nat. Photon. ***14***, 748–754, https://doi.org/10.1038/s41566-020-00712-8.
23. Allaria, E., Appio, R., Badano, L., et al. (2012). Highly coherent and stable pulses from the FERMI seeded free-electron laser in the extreme ultraviolet. Nat. Photon. ***6***, 699–704, https://doi.org/10.1038/nphoton.2012.233.
24. Zhao, Z., Wang, D., Gu, Q., et al. (2017). SXFEL: a soft X-ray free electron laser in China. Synchrotron Radiat. News ***30***, 29–33, https://doi.org/10.1080/08940886.2017.1386997.
25. Galayda, J. (2014). The Linac Coherent Light Source-II Project, In Proc. 5th International Particle Accelerator Conference (IPAC'14), Geneva, Switzerland, JACoW. Dresden, Germany.
26. Decking, W., Abeghyan, S., Abramian, P., et al. (2020). A MHz-repetition-rate hard X-ray free-electron laser driven by a superconducting linear accelerator. Nat. Photon. ***14***, 391–397, https://doi.org/10.1038/s41566- 020-0607-z.
27. Zhao, Z., Wang, D., Yang, Z., et al. (2018). SCLF: an 8-GeV CW SCRF Linac-based X-ray FEL facility in Shanghai, In Proc. Of International Free Electron Laser Conference (FEL'17), Geneva, Switzerland, JACoW.
28. Elias, L.R., Fairbank, W.M., Madey, J.M.J., et al. (1976). Observation of stimulated emission of radiation by relativistic electrons in a spatially periodic transverse magnetic field. Phys. Rev. Lett. ***36***, 717–720, https://doi.org/10.1103/PhysRevLett.36.717.
29. Yu, L.H. (1991). Generation of intense UV radiation by subharmonically seeded single-pass free-electron lasers. Phys. Rev. A. ***44***, 5178–5193, https://doi.org/10.1103/PhysRevA.44.5178.
30. Shvyd'ko, Y.V., Stoupin, S., Cunsolo, A., et al. (2010). High-reflectivity high-resolution X-ray crystal optics with diamonds. Nat. Phys. ***6***, 196–199, https://doi.org/10.1038/nphys1506.
31. Colson, W. (1977). Free electron Laser Theory, Doctoral dissertation (Stanford University).
32. Motz, H. (1951). Applications of the radiation from fast electron beams. J. Appl. Phys. ***22***, 527–535, https://doi.org/10.1063/1.1700002.
33. Saldin, E.L., Schneidmiller, E.A., and Yurkov, M.V. (2000). The Physics of Free Electron Lasers (Berlin, Heidelberg: Springer Berlin Heidelberg).
34. Pellegrini, C., Marinelli, A., and Reiche, S. (2016). The physics of X-ray free-electron lasers. Rev. Mod. Phys. ***88***, 015006, https://doi.org/10.1103/RevModPhys.88.015006.
35. Dattoli, G., Palma, E.D., Pagnutti, S., et al. (2018). Free electron coherent sources: from microwave to X-rays. Phys. Rep. ***739***, 1–51, https://doi.org/10.1016/j.physrep.2018.02.005.
36. Huang, Z., and Kim, K.-J. (2007). Review of X-ray free-electron laser theory. Phys. Rev. Accel. Beams ***10***, 034801, https://doi.org/10.1103/PhysRevSTAB.10.034801.
37. Feldhaus, J., Saldin, E., Schneider, J., et al. (1997). Possible application of X-ray optical elements for reducing the spectral bandwidth of an X-ray SASE FEL. Opt. Commun. ***140***, 341–352, https://doi.org/10.1016/S0030-4018(97)00163-6.
38. McNeil, B.W.J., Thompson, N.R., and Dunning, D.J. (2013). Transform-limited X-ray pulse generation from a high-brightness self-amplified spontaneous-emission free-electron laser. Phys. Rev. Lett. ***110***, 134802, https://doi.org/10.1103/PhysRevLett.110.134802.
39. Wu, J. et al. (2013). X-ray Spectra and Peak Power Control with iSASE, In 4th International Particle Accelerator Conference, JACoW Publishing.
40. Xiang, D., Ding, Y., Huang, Z., et al. (2013). Purified self-amplified spontaneous emission free-electron lasers with slippage-boosted filtering. Phys. Rev. Accel. Beams ***16***, 010703, https://doi.org/10.1103/PhysRevSTAB.16.010703.
41. Schneidmiller, E.A., and Yurkov, M.V. (2012). Harmonic lasing in X-ray free electron lasers. Phys. Rev. Accel. Beams ***15***, 080702, https://doi.org/10.1103/PhysRevSTAB.15.080702.
42. Amann, J., Berg, W., Blank, V., et al. (2012). Demonstration of self-seeding in a hard-X-ray free-electron laser. Nat. Photon. ***6***, 693, https://doi.org/10.1038/nphoton.2012.180.
43. Ratner, D., Abela, R., Amann, J., et al. (2015). Experimental demonstration of a soft X-ray self-seeded free-electron laser. Phys. Rev. Lett. ***114***, 054801, https://doi.org/10.1103/PhysRevLett.114.054801.
44. Inoue, I., Osaka, T., Hara, T., et al. (2019). Generation of narrow-band X-ray free-electron laser via reflection self-seeding. Nat. Photon. ***13***, 319–322, https://doi.org/10.1038/s41566- 019-0365-y.
45. Geloni, G., Kocharyan, V., and Saldin, E. (2011). A novel self-seeding scheme for hard X-ray FELs. J. Mod. Opt. ***58***, 1391–1403, https://doi.org/10.1080/09500340.2011.586473.
46. Zhang, H., Li, K., Yan, J., et al. (2018). Atomic inner-shell radiation seeded free-electron lasers. Phys. Rev. Accel. Beams ***21***, 070701, https://doi.org/10.1103/PhysRevAccelBeams.21.070701.
47. Yu, L.-H. (2000). High-gain harmonic-generation free-electron laser. Science ***289***, 932–934, https://doi.org/10.1126/science.289.5481.932.
48. Stupakov, G. (2009). Using the beam-echo effect for generation of short-wavelength radiation. Phys. Rev. Lett. ***102***, 074801, https://doi.org/10.1103/PhysRevLett.102.074801.
49. Xiang, D., Colby, E., Dunning, M., et al. (2010). Demonstration of the echo-enabled harmonic generation technique for short-wavelength seeded free electron lasers. Phys. Rev. Lett. ***105***, 114801, https://doi.org/10.1103/PhysRevLett.105.114801.
50. Zhao, Z.T., Wang, D., Chen, J.H., et al. (2012). First lasing of an echo-enabled harmonic generation free-electron laser. Nat. Photon. ***6***, 360–363, https://doi.org/10.1038/nphoton.2012.105.
51. Xiang, D., Colby, E., Dunning, M., et al. (2012). Evidence of high harmonics from echo-enabled harmonic generation for seeding X-ray free electron lasers. Phys. Rev. Lett. ***108***, 024802, https://doi.org/10.1103/PhysRevLett.108.024802.
52. Hemsing, E., Dunning, M., Garcia, B., et al. (2016). Echo-enabled harmonics up to the 75th order from precisely tailored electron beams. Nat. Photon. ***10***, 512–515, https://doi.org/10.1038/nphoton.2016.101.
53. Feng, C., Deng, H., Zhang, M., et al. (2019). Coherent extreme ultraviolet free-electron laser with echo-enabled harmonic generation. Phys. Rev. Accel. Beams ***22***, 050703, https://doi.org/10.1103/PhysRevAccelBeams.22.050703.
54. Rebernik Ribič, P., Abrami, A., Badano, L., et al. (2019). Coherent soft X-ray pulses from an echo-enabled harmonic generation free-electron laser. Nat. Photon. ***13***, 555–561, https://doi.org/10.1038/s41566-019-0427-1.
55. Zhou, K., Feng, C., and Wang, D. (2016). Feasibility study of generating ultra-high harmonic radiation with a single stage echo-enabled harmonic generation scheme. Nucl. Instrum. Methods Phys. Res. A ***834***, 30–35, https://doi.org/10.1016/j.nima.2016.07.021.
56. Deng, H., and Feng, C. (2013). Using off-resonance laser modulation for beam-energy-spread cooling in generation of short-wavelength radiation. Phys. Rev. Lett. ***111***, 084801, https://doi.org/10.1103/PhysRevLett.111.084801.
57. Feng, C., Deng, H., Wang, D., et al. (2014). Phase-merging enhanced harmonic generation free-electron laser. New J. Phys. ***16***, 043021, https://doi.org/10.1088/1367-2630/16/4/043021.
58. Qi, Z., Feng, C., Deng, H., et al. (2017). Parameter optimization and start-to-end simulation for the phase-merging enhanced harmonic generation free electron laser. Nucl. Instrum. Methods Phys. Res. A. ***875***, 119–124, https://doi.org/10.1016/j.nima.2017.08.059.
59. Feng, C., Zhang, T., Deng, H., et al. (2014). Three-dimensional manipulation of electron beam phase space for seeding soft X-ray free-electron lasers. Phys. Rev. Accel. Beams ***17***, 070701, https://doi.org/10.1103/PhysRevSTAB.17.070701.
60. Liu, W., and Jiao, Y. (2018). Generating Ultrashort X-Ray Pulse in a Diffraction-Limed Storage Ring by Phase-Merging Enhanced Harmonic Generation with Normal Modulator, In Proc. 9th International Particle Accelerator Conference (IPAC'18), Geneva, Switzerland, JACoW Publishing. Vancouver, BC, Canada.
61. Jia, Q., and Li, H. (2017). Normal planar undulators doubling as transverse gradient undulators. Phys. Rev. Accel. Beams ***20***, 020707, https://doi.org/10.1103/PhysRevAccelBeams.20.020707.
62. Zhao, Z., Li, H., and Jia, Q. (2017). Phase-merging enhanced harmonic generation free-electron laser with a normal modulator. J. Synchrotron Radiat. ***24***, 906–911, https://doi.org/10.1107/S1600577517008402.
63. Yu, L.-H., and Ben-Zvi, I. (1997). High-gain harmonic generation of soft X-rays with the "fresh bunch" technique. Nucl. Instrum. Methods Phys. Res. A ***393***, 96–99, https://doi.org/10.1016/S0168-9002(97)00435-X.
64. Wang, G.-L., Zhang, W.-Q., Yang, X.-M., et al. (2016). Fully coherent hard X-ray generation by two-stage phase-merging enhanced harmonic generation. Chin. Phys. C ***40***, 098101, https://doi.org/10.1088/1674-1137/40/9/098101.
65. Liu, B., Li, W.B., Chen, J.H., et al. (2013). Demonstration of a widely-tunable and fully-coherent high-gain harmonic-generation free-electron laser. Phys. Rev. Accel. Beams ***16***, 020704, https://doi.org/10.1103/PhysRevSTAB.16.020704.
66. Allaria, E., Castronovo, D., Cinquegrana, P., et al. (2013). Two-stage seeded soft-X-ray free-electron laser. Nat. Photon. ***7***, 913–918, https://doi.org/10.1038/nphoton.2013.277.
67. Kim, K.-J., Shvyd'ko, Y., and Reiche, S. (2008). A proposal for an X-ray free-electron laser oscillator with an energy-recovery linac. Phys. Rev. Lett. ***100***, 244802, https://doi.org/10.1103/PhysRevLett.100.244802.
68. Huang, Z., and Ruth, R.D. (2006). Fully coherent X-ray pulses from a regenerative-amplifier free-electron laser. Phys. Rev. Lett. ***96***, 144801, https://doi.org/10.1103/PhysRevLett.96.144801.
69. Shvyd'ko, Y. (2019). Output coupling from X-ray free-electron laser cavities with intracavity beam splitters. Phys. Rev. Accel. Beams ***22***, 100703, https://doi.org/10.1103/PhysRevAccelBeams.22.100703.
70. Huang, N.-S., Li, K., and Deng, H.-X. (2019). BRIGHT: the three-dimensional X-ray crystal Bragg diffraction code. Nucl. Sci. Tech. ***30***, 39, https://doi.org/10.1007/s41365-019-0559-5.

71. Huang, N., and Deng, H. (2020a). Thermal loading on crystals in an X-ray free-electron laser oscillator. Phys. Rev. Accel. Beams ***23***, 090704, https://doi.org/10.1103/PhysRevAccelBeams.23.090704.
72. Li, K., Song, M., and Deng, H. (2017). Simplified model for fast optimization of a free-electron laser oscillator. Phys. Rev. Accel. Beams ***20***, 030702, https://doi.org/10.1103/PhysRevAccelBeams.20.030702.
73. Li, K., and Deng, H. (2018). Gain-guided X-ray free-electron laser oscillator. Appl. Phys. Lett. ***113***, 061106, https://doi.org/10.1063/1.5037180.
74. Dai, J., Deng, H., and Dai, Z. (2012). Proposal for an X-ray free electron laser oscillator with intermediate energy electron beam. Phys. Rev. Lett. ***108***, 034802, https://doi.org/10.1103/PhysRevLett.108.034802.
75. Ciocci, F., Dattoli, G., De Angelis, A., et al. (1995). Design considerations on a high-power VUV FEL. IEEE J. Quan. Electron. ***31***, 1242–1252, https://doi.org/10.1109/3.391087.
76. Dattoli, G., and Ottaviani, P.L. (1999). Design considerations for X-ray free electron lasers. J. Appl. Phys. ***86***, 5331–5336, https://doi.org/10.1063/1.371528.
77. Gandhi, P., Penn, G., Reinsch, M., et al. (2013). Oscillator seeding of a high gain harmonic generation free electron laser in a radiator-first configuration. Phys. Rev. Accel. Beams ***16***, 020703, https://doi.org/10.1103/PhysRevSTAB.16.020703.
78. Ackermann, S., Faatz, B., Grattoni, V., et al. (2020). Novel method for the generation of stable radiation from free-electron lasers at high repetition rates. Phys. Rev. Accel. Beams ***23***, 071302, https://doi.org/10.1103/PhysRevAccelBeams.23.071302.
79. Li, K., Yan, J., Feng, C., et al. (2018). High brightness fully coherent X-ray amplifier seeded by a free-electron laser oscillator. Phys. Rev. Accel. Beams ***21***, 040702, https://doi.org/10.1103/PhysRevAccelBeams.21.040702.
80. Li, K., and Deng, H. (2017). Gain cascading scheme of a free-electron-laser oscillator. Phys. Rev. Accel. Beams ***20***, 110703, https://doi.org/10.1103/PhysRevAccelBeams.20.110703.
81. Huang, N., Li, K., and Deng, H. (2020). Polarization control of an X-ray free electron laser oscillator. Phys. Rev. Accel. Beams ***23***, 030702, https://doi.org/10.1103/PhysRevAccelBeams.23.030702.
82. Huang, N., and Deng, H. (2020b). Generating X-Rays with Orbital Angular Momentum in Free-Electron Laser Oscillator (arXiv), 2007.08773.
83. Halavanau, A., Benediktovitch, A., Lutman, A.A., et al. (2020). Population inversion X-ray laser oscillator. Proc. Natl. Acad. Sci. U S A ***117***, 15511–15516, https://doi.org/10.1073/pnas.2005360117.
84. Bostedt, C., Boutet, S., Fritz, D.M., et al. (2016). Linac coherent light source: the first five years. Rev. Mod. Phys. ***88***, 015007, https://doi.org/10.1103/RevModPhys.88.015007.
85. Feng, C., and Deng, H.-X. (2018). Review of fully coherent free-electron lasers. Nucl. Sci. Tech. ***29***, 160, https://doi.org/10.1007/s41365-018-0490-1.
86. Seddon, E.A., Clarke, J.A., Dunning, D.J., et al. (2017). Short-wavelength free-electron laser sources and science: a review. Rep. Prog. Phys. ***80***, 115901, https://doi.org/10.1088/1361-6633/aa7cca.
87. Tono, K., Hara, T., Yabashi, M., et al. (2019). Multiple-beamline operation of SACLA. J. Synchrotron Radiat. ***26***, 595–602, https://doi.org/10.1107/S1600577519001607.
88. Rossbach, J., Schneider, J.R., and Wurth, W. (2019). 10 years of pioneering X-ray science at the Free-Electron Laser FLASH at DESY. Phys. Rep. ***808***, 1–74, https://doi.org/10.1016/j.physrep.2019.02.002.
89. Yong, H., Zotev, N., Ruddock, J.M., et al. (2020). Observation of the molecular response to light upon photoexcitation. Nat. Commun. ***11***, 2157, https://doi.org/10.1038/s41467-020-15680-4.
90. Loh, Z.-H., Doumy, G., Arnold, C., et al. (2020). Observation of the fastest chemical processes in the radiolysis of water. Science ***367***, 179–182, https://doi.org/10.1126/science.aaz4740.
91. Schnorr, K., Senftleben, A., Kurka, M., et al. (2014). Electron rearrangement dynamics in dissociating $I2^{n+}$ molecules accessed by extreme ultraviolet pump-probe experiments. Phys. Rev. Lett. ***113***, 073001, https://doi.org/10.1103/PhysRevLett.113.073001.
92. Rudenko, A., Inhester, L., Hanasaki, K., et al. (2017). Femtosecond response of polyatomic molecules to ultra-intense hard X-rays. Nature ***546***, 129–132, https://doi.org/10.1038/nature22373.
93. Chapman, H.N., Barty, A., Bogan, M.J., et al. (2006). Femtosecond diffractive imaging with a soft-X-ray free-electron laser. Nat. Phys. ***2***, 839–843, https://doi.org/10.1038/nphys461.
94. Son, S.-K., Young, L., and Santra, R. (2011). Impact of hollow-atom formation on coherent X-ray scattering at high intensity. Phys. Rev. A ***83***, 033402, https://doi.org/10.1103/PhysRevA.83.033402.
95. Young, L., Kanter, E.P., Krẃssig, B., et al. (2010). Femtosecond electronic response of atoms to ultra-intense X-rays. Nature ***466***, 56–61, https://doi.org/10.1038/nature09177.
96. Tamasaku, K., Shigemasa, E., Inubushi, Y., et al. (2014). X-ray two-photon absorption competing against single and sequential multiphoton processes. Nat. Photon. ***8***, 313–316, https://doi.org/10.1038/nphoton.2014.10.
97. Glover, T.E., Fritz, D.M., Cammarata, M., et al. (2012). X-ray and optical wave mixing. Nature ***488***, 603–608, https://doi.org/10.1038/nature11340.
98. Weninger, C., Purvis, M., Ryan, D., et al. (2013). Stimulated electronic X-ray Raman scattering. Phys. Rev. Lett. ***111***, 233902, https://doi.org/10.1103/PhysRevLett.111.233902.
99. Rohringer, N., Ryan, D., London, R.A., et al. (2012). Atomic inner-shell X-ray laser at 1.46 nanometres pumped by an X-ray free-electron laser. Nature ***481***, 488–491, https://doi.org/10.1038/nature10721.
100. Miao, J., Charalambous, P., Kirz, J., et al. (1999). Extending the methodology of X-ray crystallography to allow imaging of micrometre-sized non-crystalline specimens. Nature ***400***, 342–344, https://doi.org/10.1038/22498.
101. Boutet, S., Lomb, L., Williams, G.J., et al. (2012). High-resolution protein structure determination by serial femtosecond crystallography. Science ***337***, 362–364, https://doi.org/10.1126/science.1217737.
102. Tenboer, J., Basu, S., Zatsepin, N., et al. (2014). Time-resolved serial crystallography captures high-resolution intermediates of photoactive yellow protein. Science ***346***, 1242–1246, https://doi.org/10.1126/science.1259357.
103. Aquila, A., Barty, A., Bostedt, C., et al. (2015). The linac coherent light source single particle imaging road map. Struct. Dyn. ***2***, 041701, https://doi.org/10.1063/1.4918726.
104. Seibert, M.M., Ekeberg, T., Maia, F.R.N.C., et al. (2011). Single mimivirus particles intercepted and imaged with an X-ray laser. Nature ***470***, 78–81, https://doi.org/10.1038/nature09748.
105. Ekeberg, T., Svenda, M., Abergel, C., et al. (2015). Three-dimensional reconstruction of the giant mimivirus particle with an X-ray free-electron laser. Phys. Rev. Lett. ***114***, 098102, https://doi.org/10.1103/PhysRevLett.114.098102.
106. Hosseinizadeh, A., Mashayekhi, G., Copperman, J., et al. (2017). Conformational landscape of a virus by single-particle X-ray scattering. Nat. Methods ***14***, 877–881, https://doi.org/10.1038/nmeth.4395.
107. Poudyal, I., Schmidt, M., and Schwander, P. (2020). Single-particle imaging by X-ray free-electron lasers. How many snapshots are needed? Struct. Dyn. ***7***, 024102, https://doi.org/10.1063/1.5144516.
108. Kimura, T., Joti, Y., Shibuya, A., et al. (2014). Imaging live cell in micro-liquid enclosure by X-ray laser diffraction. Nat. Commun. ***5***, 3052, https://doi.org/10.1038/ncomms4052.
109. van der Schot, G., Svenda, M., Maia, F.R.N.C., et al. (2015). Imaging single cells in a beam of live cyanobacteria with an X-ray laser. Nat. Commun. ***6***, 5704, https://doi.org/10.1038/ncomms6704.
110. Clark, J.N., Beitra, L., Xiong, G., et al. (2015). Imaging transient melting of a nanocrystal using an X-ray laser. Proc. Natl. Acad. Sci. U S A ***112***, 7444–7448, https://doi.org/10.1073/pnas.1417678112.
111. Ihm, Y., Cho, D.H., Sung, D., et al. (2019). Direct observation of picosecond melting and disintegration of metallic nanoparticles. Nat. Commun. ***10***, 2411, https://doi.org/10.1038/s41467-019- 10328-4.
112. Korn, G., Bulanov, S.V., Chambaret, J.-P., et al. (2010). Extreme light infrastructure (ELI): physics and lasers at the ultra-intense frontier. In Conference on Lasers and Electro-Optics 2010 (OSA) http://www.osapublishing.org/abstract.cfm?URI=CLEO-2010-JThG2.
113. Papadopoulos, D., Zou, J., Blanc, C.L., et al. (2016). The Apollon 10 PW laser: experimental and theoretical investigation of the temporal characteristics. High Power Laser Sci. Eng. ***4***, e34, https://doi.org/10.1017/hpl.2016.34.
114. Hernandez-Gomez, C., Blake, S.P., Chekhlov, O., et al. (2010). The Vulcan 10 PW project. J. Phys. Conf. Ser. ***244***, 032006, https://doi.org/10.1088/1742- 6596/244/3/032006.
115. Li, W., Gan, Z., Yu, L., et al. (2018). 339 J high-energy Ti:sapphire chirped-pulse amplifier for 10 PW laser facility. Opt. Lett. ***43***, 5681, https://doi.org/10.1364/OL.43.005681.
116. Heisenberg, W., and Euler, H. (1936). Folgerungen aus der Diracschen Theorie des Positrons. Z. Physik ***98***, 714–732, https://doi.org/10.1007/BF01343663.
117. Heinzl, T., Liesfeld, B., Amthor, K.-U., et al. (2006). On the observation of vacuum birefringence. Opt. Commun. ***267***, 318–321, https://doi.org/10.1016/j.optcom.2006.06.053.
118. Shen, B., Bu, Z., Xu, J., et al. (2018). Exploring vacuum birefringence based on a 100 PW laser and an X-ray free electron laser beam. Plasma Phys. Control Fusion ***60***, 044002, https://doi.org/10.1088/1361-6587/aaa7fb.
119. Marx, B., Schulze, K.S., Uschmann, I., et al. (2013). High-precision X-ray polarimetry. Phys. Rev. Lett. ***110***, 254801, https://doi.org/10.1103/PhysRevLett.110.254801.
120. Ding, Y., Brachmann, A., Decker, F.-J., et al. (2009). Measurements and simulations of ultralow emittance and ultrashort electron beams in the linac coherent light source. Phys. Rev. Lett. ***102***, 254801, https://doi.org/10.1103/PhysRevLett.102.254801.
121. Ding, Y., Behrens, C., Coffee, R., et al. (2015). Generating femtosecond X-ray pulses using an emittance-spoiling foil in free-electron lasers. Appl. Phys. Lett. ***107***, 191104, https://doi.org/10.1063/1.4935429.
122. Zholents, A.A., and Fawley, W.M. (2004). Proposal for intense attosecond radiation from an X-ray free-electron laser. Phys. Rev. Lett. ***92***, 224801, https://doi.org/10.1103/PhysRevLett.92.224801.
123. Qi, Z., Feng, C., Deng, H., et al. (2018). Generating attosecond X-ray pulses through an angular dispersion enhanced self-amplified spontaneous emission free electron laser. Phys. Rev. Accel. Beams ***21***, 120703, https://doi.org/10.1103/PhysRevAccelBeams.21.120703.

124. MacArthur, J.P., Duris, J., Zhang, Z., et al. (2019). Phase-stable self-modulation of an electron beam in a magnetic wiggler. Phys. Rev. Lett. ***123***, 214801, https://doi.org/10.1103/PhysRevLett.123.214801.
125. Duris, J., Li, S., Driver, T., et al. (2020). Tunable isolated attosecond X-ray pulses with gigawatt peak power from a free-electron laser. Nat. Photon. ***14***, 30–36, https://doi.org/10.1038/s41566-019- 0549-5.
126. Saldin, E.L., Schneidmiller, E.A., and Yurkov, M.V. (2006). Self-amplified spontaneous emission FEL with energy-chirped electron beam and its application for generation of attosecond X-ray pulses. Phys. Rev. Accel. Beams ***9***, 050702, https://doi.org/10.1103/PhysRevSTAB.9.050702.
127. Tanaka, T. (2013). Proposal for a pulse-compression scheme in X-ray free-electron lasers to generate a multiterawatt, attosecond X-ray pulse. Phys. Rev. Lett. ***110***, 084801, https://doi.org/10.1103/PhysRevLett.110.084801.
128. Parc, Y., Shim, C., and Kim, D. (2018). Toward the generation of an isolated TW-attosecond X-ray pulse in XFEL. Appl. Sci. ***8***, 1588, https://doi.org/10.3390/app8091588.
129. Fawley, W.M., Huang, Z., Kim, K.-J., et al. (2002). Tapered undulators for SASE FELs. Nucl. Instrum. Methods Phys. Res. A ***483***, 537–541, https://doi.org/10.1016/S0168-9002(02)00377-7.
130. Jiao, Y., Wu, J., Cai, Y., et al. (2012). Modeling and multidimensional optimization of a tapered free electron laser. Phys. Rev. Accel. Beams ***15***, 050704, https://doi.org/10.1103/PhysRevSTAB.15.050704.
131. Wu, J., Hu, N., Setiawan, H., et al. (2017). Multi-dimensional optimization of a terawatt seeded tapered free electron laser with a multi-objective genetic algorithm. Nucl. Instrum. Methods Phys. Res. A. ***846***, 56–63, https://doi.org/10.1016/j.nima.2016.11.035.
132. Marinelli, A., Ratner, D., Lutman, A., et al. (2015). High-intensity double-pulse X-ray free-electron laser. Nat. Commun. ***6***, 6369, https://doi.org/10.1038/ncomms7369.
133. Lutman, A.A., Coffee, R., Ding, Y., et al. (2013). Experimental demonstration of femtosecond two-color X-ray free-electron lasers. Phys. Rev. Lett. ***110***, 134801, https://doi.org/10.1103/PhysRevLett.110.134801.
134. Marinelli, A., Lutman, A.A., Wu, J., et al. (2013). Multicolor operation and spectral control in a gain-modulated X-ray free-electron laser. Phys. Rev. Lett. ***111***, 134801, https://doi.org/10.1103/PhysRevLett.111.134801.
135. Hara, T., Inubushi, Y., Katayama, T., et al. (2013). Two-colour hard X-ray free-electron laser with wide tunability. Nat. Commun. ***4***, 2919, https://doi.org/10.1038/ncomms3919.
136. Lutman, A.A., Maxwell, T.J., MacArthur, J.P., et al. (2016). Fresh-slice multicolour X-ray free-electron lasers. Nat. Photon. ***10***, 745–750, https://doi.org/10.1038/nphoton.2016.201.
137. Lutman, A.A., Decker, F.-J., Arthur, J., et al. (2014). Demonstration of single-crystal self-seeded two-color X-ray free-electron lasers. Phys. Rev. Lett. ***113***, 254801, https://doi.org/10.1103/PhysRevLett.113.254801.
138. Deng, H., Zhang, T., Feng, L., et al. (2014). Polarization switching demonstration using crossed-planar undulators in a seeded free-electron laser. Phys. Rev. Accel. Beams ***17***, 020704, https://doi.org/10.1103/PhysRevSTAB.17.020704.
139. Ferrari, E., Allaria, E., Buck, J., et al. (2015). Single shot polarization characterization of XUV FEL pulses from crossed polarized undulators. Sci. Rep. ***5***, 13531, https://doi.org/10.1038/srep13531.
140. Allaria, E., Diviacco, B., Callegari, C., et al. (2014). Control of the polarization of a vacuum-ultraviolet, high-gain, free-electron laser. Phys. Rev. X ***4***, 041040, https://doi.org/10.1103/PhysRevX.4.041040.
141. Lutman, A.A., MacArthur, J.P., Ilchen, M., et al. (2016). Polarization control in an X-ray free-electron laser. Nat. Photon. ***10***, 468–472, https://doi.org/10.1038/nphoton.2016.79.
142. Hara, T., Tamasaku, K., Asaka, T., et al. (2013). Time-interleaved multienergy acceleration for an X-ray free-electron laser facility. Phys. Rev. Accel. Beams ***16***, 080701, https://doi.org/10.1103/PhysRevSTAB.16.080701.
143. Yan, J., and Deng, H. (2019). Multi-beam-energy operation for the continuous-wave X-ray free electron laser. Phys. Rev. Accel. Beams ***22***, 090701, https://doi.org/10.1103/PhysRevAccelBeams.22.090701.
144. Zhang, Z., Ding, Y., Adolphsen, C., et al. (2019). Multienergy operation analysis in a superconducting linac based on off-frequency detune method. Phys. Rev. Accel. Beams ***22***, 110702, https://doi.org/10.1103/PhysRevAccelBeams.22.110702.
145. Petrillo, V., Opromolla, M., Bacci, A., et al. (2020). Coherent, high repetition rate tender X-ray free-electron laser seeded by an extreme ultra-violet free-electron laser oscillator. New J. Phys. ***22***, 073058, https://doi.org/10.1088/1367-2630/ab9bbf.
146. Yan, J., Gao, Z., Qi, Z., et al. (2021). Self-amplification of coherent energy modulation in seeded free-electron lasers. Phys. Rev. Lett. ***126***, 084801, https://doi.org/10.1103/PhysRevLett.126.084801.
147. Kim, K.-J., Bisognano, J., Garren, A., et al. (1985). Issues in storage-ring design for operation of high-gain FEL. Nucl. Instrum. Methods Phys. Res. A ***239***, 54–61, https://doi.org/10.1016/0168- 9002(85)90698-9.
148. Dattoli, G., Palma, E.D., Petralia, A., et al. (2012). SASE FEL storage ring. IEEE J. Quan. Electron. ***48***, 1259–1264, https://doi.org/10.1109/JQE.2012.2208733.
149. Mitri, S.D., and Cornacchia, M. (2015). Operating synchrotron light sources with a high gain free electron laser. New J. Phys. ***17***, 113006, https://doi.org/10.1088/1367-2630/17/11/113006.
150. Cai, Y., Ding, Y., Hettel, R., et al. (2013). An X-ray free electron laser driven by an ultimate storage ring. Synchrotron Radiat. News ***26***, 39–41, https://doi.org/10.1080/08940886.2013.791216.
151. De Ninno, G., Allaria, E., Coreno, M., et al. (2008). Generation of ultrashort coherent vacuum ultraviolet pulses using electron storage rings: a new bright light source for experiments. Phys. Rev. Lett. ***101***, 053902, https://doi.org/10.1103/PhysRevLett.101.053902.
152. Evain, C., Loulergue, A., Nadji, A., et al. (2012). Soft X-ray femtosecond coherent undulator radiation in a storage ring. New J. Phys. ***14***, 023003, https://doi.org/10.1088/1367-2630/14/2/023003.
153. Liu, W.-H., Zhou, G.-Q., and Jiao, Y. (2018). Generating femtosecond coherent X-ray pulses in a diffraction-limited storage ring with the echo-enabled harmonic generation scheme. Nucl. Sci. Tech. ***29***, 143, https://doi.org/10.1007/s41365-018-0476-z.
154. Xiang, D., and Wan, W. (2010). Generating ultrashort coherent soft X-ray radiation in storage rings using angular-modulated electron beams. Phys. Rev. Lett. ***104***, 084803, https://doi.org/10.1103/PhysRevLett.104.084803.
155. Feng, C., Xiang, D., Deng, H., et al. (2015). Generating intense fully coherent soft X-ray radiation based on a laser-plasma accelerator. Opt. Express ***23***, 14993, https://doi.org/10.1364/OE.23.014993.
156. Feng, C., and Zhao, Z. (2017). A storage ring based free-electron laser for generating ultrashort coherent EUV and X-ray radiation. Sci. Rep. ***7***, 4724, https://doi.org/10.1038/s41598-017-04962-5.
157. Wang, X., Feng, C., Liu, T., et al. (2019). Angular dispersion enhanced prebunch for seeding ultrashort and coherent EUV and soft X-ray free-electron laser in storage rings. J. Synchrotron Radiat. ***26***, 677–684, https://doi.org/10.1107/S1600577519002674.
158. Ratner, D.F., and Chao, A.W. (2010). Steady-state microbunching in a storage ring for generating coherent radiation. Phys. Rev. Lett. ***105***, 154801, https://doi.org/10.1103/PhysRevLett.105.154801.
159. Deng, X.J., Chao, A.W., Feikes, J., et al. (2020). Single-particle dynamics of microbunching. Phys. Rev. Accel. Beams ***23***, 044002, https://doi.org/10.1103/PhysRevAccelBeams.23.044002.
160. Deng, X., Chao, A., Feikes, J., et al. (2021). Experimental demonstration of the mechanism of steady-state microbunching. Nature ***590***, 576–579, https://doi.org/10.1038/s41586- 021-03203-0.
161. Esarey, E., Schroeder, C.B., and Leemans, W.P. (2009). Physics of laser-driven plasma-based electron accelerators. Rev. Mod. Phys. ***81***, 1229–1285, https://doi.org/10.1103/RevModPhys.81.1229.
162. Li, F., Hua, J.F., Xu, X.L., et al. (2013). Generating high-brightness electron beams via ionization injection by transverse colliding lasers in a plasma-wakefield accelerator. Phys. Rev. Lett. ***111***, 015003, https://doi.org/10.1103/PhysRevLett.111.015003.
163. Couprie, M.E., Labat, M., Evain, C., et al. (2016). An application of laser "plasma acceleration: towards a free-electron laser amplification. Plasma Phys. Control Fusion ***58***, 034020, https://doi.org/10.1088/0741-3335/58/3/034020.
164. Xu, X.L., Li, F., An, W., et al. (2017). High quality electron bunch generation using a longitudinal density-tailored plasma-based accelerator in the three-dimensional blowout regime. Phys. Rev. Accel. Beams ***20***, 111303, https://doi.org/10.1103/PhysRevAccelBeams.20.111303.
165. Xu, X.L., Hua, J.F., Wu, Y.P., et al. (2016). Physics of phase space matching for staging plasma and traditional accelerator components using longitudinally tailored plasma profiles. Phys. Rev. Lett. ***116***, 124801, https://doi.org/10.1103/PhysRevLett.116.124801.
166. Wu, Y.P., Hua, J.F., Zhou, Z., et al. (2019). Phase space dynamics of a plasma wakefield dechirper for energy spread reduction. Phys. Rev. Lett. ***122***, 204804, https://doi.org/10.1103/PhysRevLett.122.204804.
167. D'Arcy, R., Wesch, S., Aschikhin, A., et al. (2019). Tunable plasma-based energy dechirper. Phys. Rev. Lett. ***122***, 034801, https://doi.org/10.1103/PhysRevLett.122.034801.
168. Wu, Y., Hua, J., Pai, C.-H., et al. (2019). Near-ideal dechirper for plasma-based electron and positron acceleration using a hollow channel plasma. Phys. Rev. Appl. ***12***, 064011, https://doi.org/10.1103/PhysRevApplied.12.064011.
169. Emma, P., Huang, Z., Kim, K.-J., et al. (2006). Transverse-to-longitudinal emittance exchange to improve performance of high-gain free-electron lasers. Phys. Rev. Accel. Beams ***9***, 100702, https://doi.org/10.1103/PhysRevSTAB.9.100702.
170. Maier, A.R., Meseck, A., Reiche, S., et al. (2012). Demonstration scheme for a laser-plasma-driven free-electron laser. Phys. Rev. X ***2***, 031019, https://doi.org/10.1103/PhysRevX.2.031019.
171. Huang, Z., Ding, Y., and Schroeder, C.B. (2012). Compact X-ray free-electron laser from a laser-plasma accelerator using a transverse-gradient undulator. Phys. Rev. Lett. ***109***, 204801, https://doi.org/10.1103/PhysRevLett.109.204801.

172. Ciocci, F., Dattoli, G., and Sabia, E. (2015). Transverse gradient undulators and FEL operating with large energy spread. Opt. Commun. ***356***, 582–588, https://doi.org/10.1016/j.optcom.2015.08.053.

ACKNOWLEDGMENTS

The authors are grateful to Meng Zhang, Tao Liu, Kaishang Zhou, Zheng Qi, Guanglei Wang, Jiawei Yan, Chao Feng, Kai Li, Liangliang Ji, Yi Jiao, Jiadong Fan, Huaidong Jiang, Yipeng Wu, and Xiujie Deng for helpful discussions and useful assistance in the preparation of the contents and figures. This work was supported by the National Key Research and Development Program of China (2018YFE0103100, 2016YFA0401900) and the National Natural Science Foundation of China (11935020, 11775293). The SXFEL and SHINE projects are supported by the Chinese Central Government and the Shanghai Government.

AUTHOR CONTRIBUTIONS

N.H. and H.D. wrote the manuscript. B.L. and D.W. helped with the writing of the manuscript. H.D. organized and revised the manuscript. Z.Z. supervised and instructed on the manuscript. All authors read and approved the final manuscript.

DECLARATION OF INTERESTS

The authors declare no competing interests.

LEAD CONTACT WEBSITES

https://www.researchgate.net/profile/Haixiao-Deng.